

AperTO - Archivio Istituzionale Open Access dell'Università di Torino

Investigation of squalene-doxorubicin distribution and interactions within single cancer cell using Raman microspectroscopy

This is a pre print version of the following article:

Original Citation:

Availability:

This version is available <http://hdl.handle.net/2318/1792820> since 2021-07-05T15:01:16Z

Published version:

DOI:10.1016/j.nano.2021.102404

Terms of use:

Open Access

Anyone can freely access the full text of works made available as "Open Access". Works made available under a Creative Commons license can be used according to the terms and conditions of said license. Use of all other works requires consent of the right holder (author or publisher) if not exempted from copyright protection by the applicable law.

(Article begins on next page)

Nanomedicine: Nanotechnology, Biology, and Medicine

Investigation of squalene-doxorubicin distribution and interactions within single cancer cell using Raman microspectroscopy

--Manuscript Draft--

Manuscript Number:	JN2020930R1
Article Type:	Original Article
Keywords:	Raman microspectroscopy, cancer cells, squalenoylated doxorubicin nanoparticles
Corresponding Author:	Abdelilah BELJEBBAR, PhD Université de Reims champagne Ardenne Reims, FRANCE
First Author:	Hassan Rammal, PhD
Order of Authors:	Hassan Rammal, PhD Almar Al Assaad, PhD student Franco Dosio, Associate professor Barbara Stella, Professor Andrei Maksimenko, PhD Simona Mura, Associate professor Laurence Van-Gulick, PhD student Maité Callewaert, Associate Professor Didier Desmaële, Professor Patrick Couvreur, Professor Hamid Morjani, Professor Abdelilah BELJEBBAR, PhD
Abstract:	<p>Intracellular distribution of doxorubicin (DOX) and its squalenoylated (SQ-DOX) nanoparticles (NPs) form in murine lung carcinoma M109 and human breast carcinoma MDA-MB-231 cells were investigated by Raman microspectroscopy. Pharmacological data showed that DOX induced higher cytotoxic effect than SQ-DOX NPs. Raman data were obtained using single-point measurements and imaging on the whole cell areas. These data showed that after DOX treatment at 1 μM, the spectral features of DOX were not detected in the M109 cell cytoplasm and nucleus. However, the intracellular distribution of SQ-DOX NPs was higher than DOX in the same conditions. In addition, SQ-DOX NPs were localized into both cell cytoplasm and nucleus. After 5 μM treatment, Raman bands of DOX at 1211 and 1241 cm^{-1} were detected in the nucleus. Moreover, the intensity ratio of these bands decreased, indicating DOX intercalation into DNA. However, after treatment with SQ-DOX NPs, the intensity of these Raman bands increased. Interestingly, with SQ-DOX NPs, the intensity of 1210/1241 cm^{-1} ratio was higher suggesting a lower fraction of intercalated DOX in DNA and higher amount of non-hydrolyzed SQ-DOX. Raman imaging data confirm this subcellular localization of these drugs in both M109 and MDA-MB-231 cells. These finding brings new insights to the cellular characterization of anticancer drugs at the molecular level, particularly in the field of nanomedicine.</p>

March 7th, 2021

Cover Letter

Re: Submission of revised manuscript.

Dear **Editor-in-Chief**,

We thank the *Nanomedicine: Nanotechnology, Biology, and Medicine* in giving this work a chance to be reviewed. All the reviewer suggestions were taken into account to improve our manuscript. Please find enclosed the revised manuscript with highlighted changes. We hope that our admittedly lengthy comments, and changes to the manuscript render the study suitable for publication. Please note that this manuscript was initially prepared in a highly condensed fashion. Each comment of the reviewers required some additional text and figure.

Title: Investigation of squalene-doxorubicin distribution and interactions within single cancer cell using Raman microspectroscopy

Authors: H. Rammal, A. Al Assaad, F. Dosio, B. Stella, A. Maksimenko, S. Mura, L. Van Gulick, M. Callewaert, D. Desmaële, P. Couvreur, H. Morjani, A. Beljebbar

The reviewers' suggestions required additional experiments to validate this study on another cell line as well as the acquisition and processing of Raman images. A. Al Assaad carried out these important additional experiments. We therefore decided, in agreement with all the authors, to consider that H. Rammal, A. Al Assaad were contributed equally to this work. In addition, M. Callewaert is added as co-author of this work because she participated to synthesis and characterization of the SQ-DOX NPS for the additional experiments.

We will appreciate your consideration of our revised manuscript and we look forward to receiving your response in the near future.

Sincerely,

Dr. Abdelilah Beljebbar

Response to the reviewers

We sincerely thank both reviewers for their careful reading of the manuscript and their constructive remarks. According to their suggestions, we have revised the manuscript. We have addressed the raised concerns point-by-point and listed the corresponding modifications made in the revised version of the manuscript. All the modifications are highlighted in the new version of the manuscript. We feel that the manuscript is strengthened by the suggestions of the reviewers.

Reviewer: 1

- 1. The authors should present mapping images of Raman signals and bright field imaging; it is clearer to demonstrate cellular distribution of the drug.***

As suggested by the reviewer, Raman spectral images of drugs were recorded on single M109 and MDA-MB-231 cells. These images were acquired with the same experimental conditions than single point measurements with spatial resolution of 1 μm . Data set was divided into two groups for the two drugs. Multivariate statistical analysis (PCA) was performed on two different data sets PCA was used to investigate the subcellular localization of the drugs. PCs potentially attributed to DOX or SQ-DOX were used to construct pseudo-colors score maps. Figure 8 displays the comparison between the two PCs of DOX (PC-Data1 and PC-Data2) potentially attributed to DOX or SQ-DOX and Raman spectra of DOX and SQ-DOX in aqueous solutions. Figure 9 shows the pseudo-color scores images associated to these PCs in M109 and MDA-MB-231 cells treated with DOX and SQ-DOX at concentration of 5 μM for 1 and 5 hours. These maps displayed significant differences in the localization of these drugs in the subcellular regions.

- 2. It is better to demonstrate one more cancer cell line to verify the study***

As suggested by the reviewer, this study was validated human breast carcinoma MDA-MB-231 cell line.

- 3. Some figures are not optimized, for example, Figure 6-8: many numbers are overlapped***

As noticed by the reviewers, the bands frequencies were corrected in figures 6, 7 and 8

Reviewer: 2

- 1. All experiments were performed in a single cell line, M109, which is sensitive to SQ-DOX but not to DOX in vivo. As the authors claimed that the drug response to DOX and SQ-DOX in vitro and in vivo was different in M109 cells, at least one more cell line should be investigated to support the conclusion from the M109 model.***

As suggested by the reviewer, this study was validated human breast carcinoma MDA-MB-231 cell line.

- 2. The graphical abstract and Figure 1 are very misleading. The green/red dots indicated the acquisition regions in cytoplasm/nucleus. However, the legend for Figure 1 was "Subcellular localization of DOX and SQ-DOX in single living M109 cell by Raman microspectroscopy". No information could be obtained from Figure 1 on the subcellular localization of DOX and SQ-DOX. These figures and corresponding legends should be revised to avoid the misleading.***

We completely agree with the reviewer comment. To avoid this confusion, Figure 1 was removed. However, the graphical abstract was kept as the overview of the study design applied to investigate the squalene-doxorubicin distribution and interactions within single cancer cell using Raman microspectroscopy imaging.

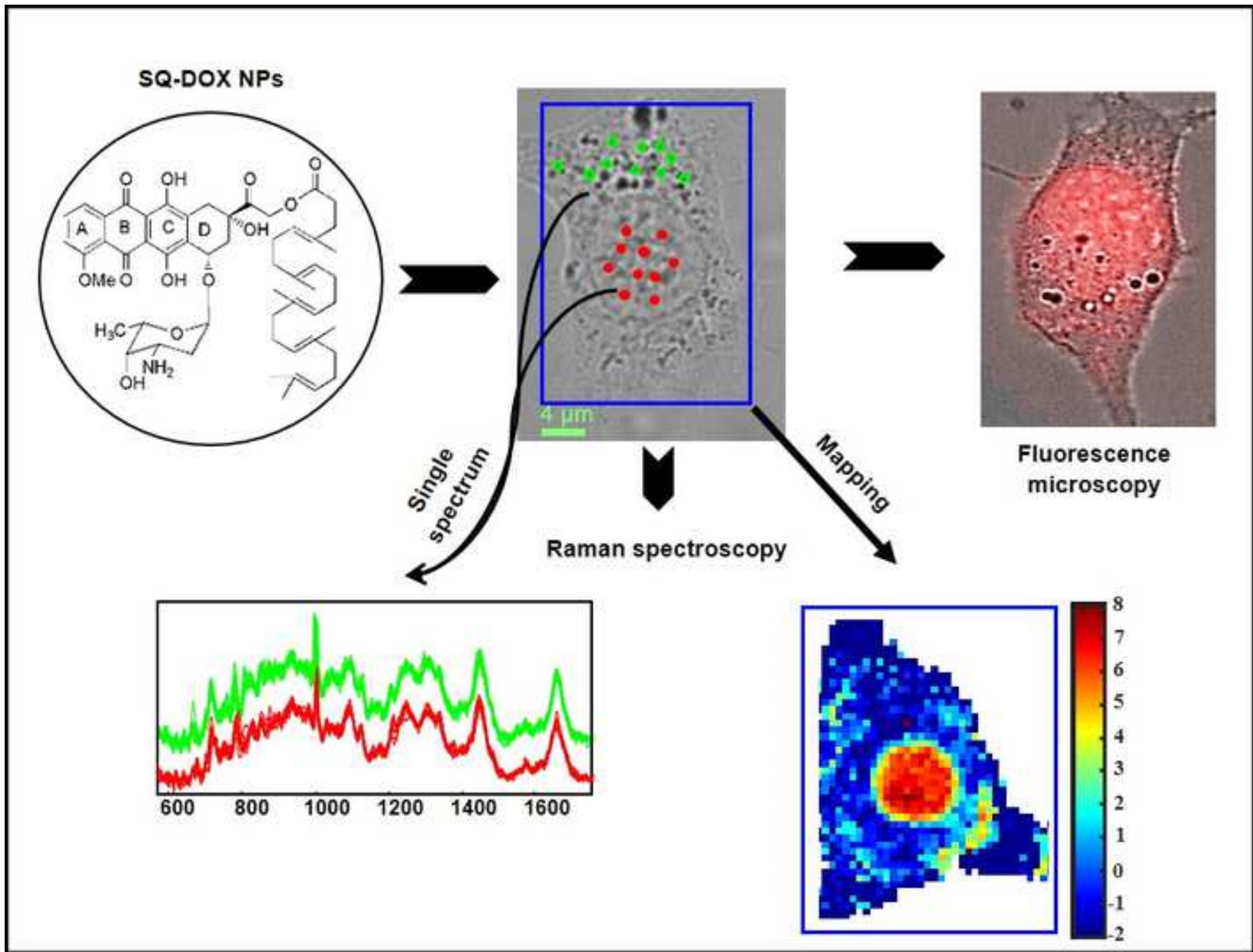
- 3. Figure 4: It is quite strange the fluorescence intensity from nuclear DOX upon DOX treatment was lower than that with SQ-DOX treatment. Please explain it.***

We modified this figure to make it clearer for the readers. Confocal fluorescence microscopy images have been improved (figure 2 instead of figure 3 previously) and fluorescence emission of the drugs from the nucleus has been quantified using Open source NIH ImageJ software (figure 3 instead of figure 4 previously). Regions-of-interest (ROIs) were selected in each nucleus. The average fluorescence intensity was determined in each ROI, for DOX and SQ-DOX NPs.

- 4. Figures 6-8: The authors should provide the distribution of DOX and SQ-DOX based on their unique spectra features using Raman microspectroscopy on a whole cell, which would help the reader for better understanding the technology.***

As suggested by the reviewer, Raman spectral images of drugs were recorded on single M109 and MDA-MB-231 cells. These images were acquired with the same experimental conditions than single point measurements with spatial resolution of 1 μm . Data set was divided into two groups for the two drugs. Multivariate statistical analysis (PCA) was performed on two different data sets PCA was used to investigate the subcellular localization of the drugs. PCs potentially attributed to DOX or SQ-DOX were used to construct pseudo-colors score maps. Figure 8 displays the comparison between the two PCs of DOX (PC-Data1 and PC-Data2) potentially attributed to DOX or SQ-DOX and Raman spectra of DOX and SQ-DOX in aqueous solutions. Figure 9 shows the pseudo-color scores images associated to these PCs in M109 and MDA-MB-231 cells treated with DOX and SQ-DOX at concentration of 5 μM for 1 and 5 hours. These maps displayed significant differences in the localization of these drugs in the subcellular regions.

Raman and fluorescence microspectroscopies were used as label-free technique to study the intracellular distribution and interaction of DOX and SQ-DOX nanoparticles in cytoplasmic and nuclear compartments of murine lung carcinoma (M109) and human breast carcinoma (MDA-MB-231) cell lines with a submicrometer spatial resolution. Our results provided simultaneously the distribution/quantification of the different forms of DOX and SQ-DOX NPs, and the identification of cellular biochemical changes induced by drug treatment.



Investigation of squalene-doxorubicin distribution and interactions within single cancer cell using Raman microspectroscopy

Hassan Rammal^{1,Ω,¶}, Almar Al Assaad^{1,Ω}, Franco Dosio², Barbara Stella², Andrei Maksimenko³, Simona. Mura³, Laurence Van Gulick¹, Maïté Callewaert⁴, Didier Desmaële³, Patrick Couvreur³, Hamid Morjani^{1#}, Abdelilah Beljebbar^{1#*}

1. Translational BioSpectroscopy, BioSpecT, EA 7506, Université de Reims, Faculté de Pharmacie, Reims, France
2. Department of Drug Science and Technology, University of Torino, 10125 Torino, Italy
3. Institut Galien Paris-Saclay CNRS UMR8612, Université Paris-Saclay, Faculté de Pharmacie, Châtenay-Malabry, France.
4. Institut de Chimie Moléculaire de Reims, ICMR - UMR 7312, Université de Reims, Faculté de Pharmacie, Reims, France

^Ω H R. and A A contributed equally to this work

[#] H M. and A B co-supervised this work

[¶] Present adress : EFOR Healthcare Paris, Biocompatibility Platform, 92300 Levallois-Perret, France.

***: Correspondence should be sent to:**

Dr. Abdelilah BELJEBBAR
Translational BioSpectroscopy, EA 7506
UFR de Pharmacie
Université de Reims Champagne-Ardenne
51, rue Cognacq-Jay,
51096 Reims CEDEX, France
Phone: (33) 3 2691-8376
Fax: (33) 3 2691-8282
E-mail: abdelilah.beljebbar@univ-reims.fr

ABSTRACT

Intracellular distribution of doxorubicin (DOX) and its squalenoylated (SQ-DOX) nanoparticles (NPs) form in murine lung carcinoma M109 and human breast carcinoma MDA-MB-231 cells were investigated by Raman microspectroscopy. Pharmacological data showed that DOX induced higher cytotoxic effect than SQ-DOX NPs. Raman data were obtained using single-point measurements and imaging on the whole cell areas. These data showed that after DOX treatment at 1 μ M, the spectral features of DOX were not detected in the M109 cell cytoplasm and nucleus. However, the intracellular distribution of SQ-DOX NPs was higher than DOX in the same conditions. In addition, SQ-DOX NPs were localized into both cell cytoplasm and nucleus. After 5 μ M treatment, Raman bands of DOX at 1211 and 1241 cm^{-1} were detected in the nucleus. Moreover, the intensity ratio of these bands decreased, indicating DOX intercalation into DNA. However, after treatment with SQ-DOX NPs, the intensity of these Raman bands increased. Interestingly, with SQ-DOX NPs, the intensity of 1210/1241 cm^{-1} ratio was higher suggesting a lower fraction of intercalated DOX in DNA and higher amount of non-hydrolyzed SQ-DOX. Raman imaging data confirm this subcellular localization of these drugs in both M109 and MDA-MB-231 cells. These finding brings new insights to the cellular characterization of anticancer drugs at the molecular level, particularly in the field of nanomedicine.

Key words: Raman microspectroscopy; cancer cells, squalenoylated doxorubicin, nanoparticles

Introduction

Cancer treatment is often limited by a lack of selectivity and toxicity(1,2). Doxorubicin (DOX) emerged as one of the most widely used anti-cancer chemotherapeutic drug (3,4). Generally, it is accepted that DOX has the ability to intercalate between the G-C base pairs (5,6) and to inhibit DNA topoisomerase II resulting in inhibition of DNA replication and cell growth (7–9). Unfortunately, the use of DOX in clinic encounters some limitations, including a lack of selectivity, cardiotoxicity and development of resistance (5,10,11).

One of the used strategies to improve antitumor efficacy, tissue distribution and pharmacokinetics of anticancer drugs is the development of nanoscale drug delivery systems (*i.e.* nanomedicine) (12). In this context, various nanocarriers of DOX have been developed (13–15). Recently, the chemical linkage of DOX to squalene (SQ), a natural lipid precursor of the cholesterol's biosynthesis, has been proposed (16). Such bioconjugate (SQ-DOX) was found to spontaneously self-assemble in water in form of nanoparticles (NPs) of 130-nm mean diameter. *In vivo*, SQ-DOX NPs were found to reduce murine pancreatic tumor growth by 95%, compared to only a 29% DOX. In M109 murine lung carcinoma, a 90% tumor inhibition was observed SQ-DOX NPs, whereas DOX was ineffective. In addition, SQ-DOX NPs were five-fold better tolerated than DOX, thus significantly reducing both cardiac and digestive toxicities (16).

A better understanding of the mechanism behind the observed anticancer efficacy, including cellular uptake, intracellular distribution and subcellular interactions is crucial to improve the benefit/risk ratio of this approach. Interestingly, near infrared Raman microspectroscopy emerged as an attractive label-free and a non-invasive methodology for monitoring the molecular information associated with the biological activity of anticancer agents (17–19). This technique has been previously used to analyze biochemical information simultaneously on both the drug and the cell components (*i.e.* DNA, RNA, proteins, and lipid content) (20–23).

1
2
3
4
5
6
7
8
9
10
11
12
13
14
15
16
17
18
19
20
21
22
23
24
25
26
27
28
29
30
31
32
33
34
35
36
37
38
39
40
41
42
43
44
45
46
47
48
49
50
51
52
53
54
55
56
57
58
59
60
61
62
63
64
65

Additionally, Raman spectroscopy has the ability to study cells in physiological conditions with high spatial resolution (24). Several studies have already investigated the effect of DOX and its interaction with DNA at the molecular and cellular levels using Raman spectroscopy (22,25–31). This technique was also used for preclinical applications such as the quantification of antineoplastic drugs in the tumor (32), and the screening of early stage cellular response to different drug treatments for improving drug efficacy and reducing toxicity (32–35).

Herein, we shed light on the potential use of Raman microspectroscopy to investigate the intracellular distribution and interaction of DOX and SQ-DOX NPs in cytoplasmic and nuclear compartments of murine lung carcinoma (M109) and human breast carcinoma (MDA-MB-321) cell lines *in vitro*.

MATERIALS AND METHODS

1. Drugs

DOX was purchased from Sigma-Aldrich (Saint-Quentin Fallavier, France). The chemical structure of DOX consists of a tetracyclic ring with the sugar daunosamine attached by a glycosidic linkage. SQ was purchased from Sigma-Aldrich. This molecule is a polyunsaturated hydrocarbon of the triterpene type. SQ-DOX was synthesized by chemical linkage of the anticancer drug DOX onto SQ (16). SQ-DOX NPs were prepared using the nanoprecipitation method. Briefly, 500 μ L of a tetrahydrofuran solution of SQ-DOX (4 mg/mL) was added dropwise under stirring (500 rpm) into 1 mL distilled water. Precipitation of the SQ-DOX NPs occurred spontaneously after evaporation of tetrahydrofuran. The diameter of the nanoparticles was determined by laser light scattering at 20 °C using a nanosizer (Zetasizer Nano ZS, Malvern Instrument, UK).

2. Cancer cell culture

The murine lung carcinoma (M109) and human breast cancer MDA-MB-231 cell lines were maintained as recommended. Briefly, M109 and MDA-MB231 cells were cultured in RPMI

1 medium 1640 and DMEM respectively supplemented with 10% heat-inactivated fetal bovine
2 serum (FBS), penicillin (100 U/mL) and streptomycin (100 µg/mL). Cells were kept in a
3 humidified atmosphere of 5% CO₂ with a medium change every two days and were routinely
4 passaged at pre-confluency using 0.05% trypsin, 0.53 mM EDTA (Invitrogen) and screened for
5 the absence of mycoplasma using PCR methods.
6
7
8
9
10

11 **3. Cytotoxicity assay**

12 M109 cells at 5×10^4 cells/ml density were allowed to adhere on 24 well plate for 24 h at 37
13 °C in a humidified atmosphere of 5% CO₂ in air. After pre-incubation, cells were washed with
14 sterile phosphates-buffered saline (PBS) and then exposed to series of concentrations of free
15 DOX or SQ-DOX NPs ranging from 0.1 nM to 1 µM for 72 h. Non treated cells were used as
16 control. For short time drug exposure, cells were exposed to series of concentrations of free
17 DOX or SQ-DOX ranging from 0.1 µM to 50 µM for 1 h. After the short time incubation, the
18 culture medium containing the drug was removed, cells were then washed and incubated with
19 a new culture medium for 72 h. Afterwards, in both protocols, cells were then washed and
20 detached using 0.05% trypsin, 0.53 mM EDTA and counted using a traditional cell Kova® slide
21 counting plate (Kova international). The inhibitory concentration 50% (IC₅₀) was defined as the
22 drug (DOX or SQ-DOX) concentration required to inhibit M109 cell growth by 50%, relative
23 to untreated controls. IC₅₀ values were estimated from the dose response curves plotted using
24 GraphPad Prism® 6 software and provided from the average of three different experiments and
25 in duplicate at each time.
26
27
28
29
30
31
32
33
34
35
36
37
38
39
40
41
42
43
44
45
46
47

48 **4. Annexin V and Caspase 3/7 analysis**

49 M109 cells at 10^5 cells/ml density were allowed to adhere on six well plate for 24 h at 37 °C in
50 a humidified atmosphere of 5% CO₂ in air. After pre-incubation, cells were then washed with
51 sterile PBS and incubated for 48 h with free DOX or SQ-DOX NPs at the concentration of 100
52 nM. After treatment, cells were harvested using trypsin-EDTA, washed two times with PBS,
53
54
55
56
57
58
59
60
61
62
63
64
65

1 and re-suspended in fresh culture medium containing 10 % serum. Cell suspensions were
2 stained using the Muse™ Annexin V and Caspase 3/7 kit (Millipore, Molsheim, France)
3
4 according to manufacturer's instructions. Data were acquired on a Muse™ Cell Analyzer
5
6 (Millipore, Molsheim, France).
7

8 9 **5. Cellular drug distribution by confocal fluorescence microscopy**

10 M109 and MDA-MB-231 cells were seeded on CaF₂ substrates, placed in petri dishes, to
11
12 achieve 40–60% confluence after 24 h at 37 °C in a humidified atmosphere of 5% CO₂ in air.
13
14 Cells were then washed with sterile PBS and incubated at 37°C with free DOX or SQ-DOX
15
16 NPs at the concentrations of 1µM for 1 hour and 5µM for 1 and 5 hours. After treatment, cells
17
18 were washed with PBS and fixed using PFA (4%), they were then analyzed by fluorescence
19
20 microscopy (Zeiss) equipped with 63X oil immersion objective and Raman microscopy.
21
22 The fluorescence of DOX was measured using excitation at 488 nm and emission at 560 nm.
23
24 We then quantified the cellular accumulation of DOX and SQ-DOX from the analysis of
25
26 fluorescence images using Open source NIH ImageJ software (Wayne Rasband, National
27
28 Institutes of Health, Bethesda, MD). Briefly, regions-of-interest (ROIs) were selected in each
29
30 nucleus by ImageJ. The average fluorescence intensity was determined in each ROI, for DOX
31
32 and SQ-DOX NPs.
33
34
35
36
37
38
39
40

41 **6. Raman microspectroscopy**

42 Raman spectra were recorded with a near infrared confocal Raman spectrometer (Labram
43
44 ARAMIS, Horiba Jobin Yvon S.A.S., France). This setup consisted of a microscope (Olympus,
45
46 BX41, France) coupled to the Raman spectrometer equipped with 600 groove/mm diffraction
47
48 grating. The microscope was equipped with a xy-motorized (Marzhauser, Germany), computer-
49
50 controlled sample stage, which enabled automatic scanning of the sample with a spatial
51
52 resolution of 1 µm. The excitation source (785 nm) was provided by diode laser (Toptica
53
54 Photonics, Germany) delivering 60 mW of laser power on the sample. This laser excitation was
55
56
57
58
59
60
61
62
63
64
65

1 focused on the single cell with water immersion NIR 100x objective (NA 1.0, Olympus,
2 France). This backscattered light was collected by the objective and was transmitted to the
3 spectrometer equipped with a Pelletier-cooled charge-coupled device detector. M109 cells and
4 MDA-MB-231 ($50 \cdot 10^3$ cells/mL /window) were seeded on previously sterilized CaF_2 windows
5 in 6-well plate 24 h before treatment. Cells were incubated with or without DOX or SQ-DOX
6 NPs at concentrations of 1 and 5 μM and placed into petri dishes for 1 h and 5 h. After
7 incubation, medium was then removed and cells were rinsed twice with sterile PBS. Cells were
8 kept in PBS for Raman acquisition. Spectra were acquired on five different cells. For each cell,
9 15 measurements were performed at two different cell compartments: nucleus and cytoplasm,
10 using a 20 seconds integration time in the $600\text{--}1800\text{ cm}^{-1}$ spectral region with a spectral
11 resolution of 4 cm^{-1} . Raman spectral images were recorded on single fixed M109 and MDA-
12 MB-231 cells non treated and treated with DOX and SQ-DOX at concentration of $5\text{ }\mu\text{M}$ for 1h
13 and 5h. These images were acquired with the same experimental conditions than single point
14 measurements with spatial resolution of $1\text{ }\mu\text{m}$.

15 Data acquisition was carried out by means of the LabSpec 5 software (Horiba Jobin Yvon
16 S.A.S. France).

17 *7. Data pretreatment*

18 Various data processing were performed on these measured data (36). After acquisition, spectra
19 were first calibrated using Raman calibration standards. The spectrum of the halogen lamp was
20 used to correct for the wavelength-dependent signal detection efficiency of the Raman setup.
21 Raman data were analyzed with custom software developed in MatLab (MathWorks, Inc.,
22 Matick, USA). All spectra were corrected for the interference background, baseline corrected
23 using a fourth order polynomial and smoothed with fifth points Savitzky-Golay algorithm in
24 order to minimize the influence of noises. The resulting spectra were then normalized using a
25 Standard Normal Variate (SNV) procedure (37).

1
2
3
4
5
6
7
8
9
10
11
12
13
14
15
16
17
18
19
20
21
22
23
24
25
26
27
28
29
30
31
32
33
34
35
36
37
38
39
40
41
42
43
44
45
46
47
48
49
50
51
52
53
54
55
56
57
58
59
60
61
62
63
64
65

Principal component analysis (PCA) was used on spectral imaging data to identify the independent sources of variation in all spectra and to reduce the number of variables describing the dataset. This procedure allowed the identification of the subsets of data that may be associated to different drug treatments. Prior to the analysis, dataset was divided into two groups according to the two different drugs. PCA was performed on each sub-dataset. PCs potentially attributed to DOX or SQ-DOX were used to construct pseudo-colors score maps. All processing on Raman spectral images was performed with Matlab (Version 9.4, MathWorks, Inc., Matick, USA).

8. Statistical analysis

ANOVA test was performed using GraphPad Prism 6 software. Statistical significance was assessed by followed by Sidak simple comparison test (* $p < 0.05$, *** $p < 0.001$).

RESULTS

1. Antitumor activity of DOX and SQ-DOX

In order to evaluate DOX and SQ-DOX NPs antitumor activity, M109 cells were pre-incubated for 24 h and then exposed to concentrations of DOX and SQ-DOX NPs ranging from 0.1 nM to 1 μ M. Dose-response assays plots allowed to calculate the drug concentration, which induces 50% cell growth inhibition (IC_{50}). After long-term treatment, DOX and SQ-DOX NPs inhibited the growth of M109 cells in a concentration-dependent manner and the calculated IC_{50} were respectively 2.6 and 18 nM (Figure 1a, table 1). After short-term treatment, DOX and SQ-DOX NPs induced also a decrease in cell growth with IC_{50} values of 0.12 and 1.2 μ M, respectively (Figure 1b, table 1). To investigate the drug-induced apoptosis, M109 cells were treated with DOX or SQ-DOX NPs at concentration of 100 nM. After 48 h incubation, Annexin-V staining revealed that SQ-DOX treatment induced 45% apoptosis, whereas DOX treatment induced 75% positive (Figure 1C) ($p < 0.001$). These results were concomitant with caspase 3/7 staining, a hallmark of the apoptosis induction, showing a higher caspase 3/7 activation upon DOX

1 treatment with 43% of positive cells compared to only 30% upon SQ-DOX treatment ($p < 0.05$)
2 (Figure 1d). While *in vivo* SQ-DOX treatment markedly inhibited M109 tumors (90% with SQ-
3 DOX vs 3% with DOX) demonstrating the efficacy of this nanomedicine even in a drug-
4 resistant tumor model, the *in vitro* results failed to highlight such effects (16). This
5 inconsistency is rather usual in the nanomedicine field, due to the slow release of the parent
6 drug from SQ-DOX nanoparticles and to their improved pharmacokinetic (*i.e.* reduced
7 clearance), reduced elimination and tumor specific biodistribution.
8
9

10 11 12 13 14 15 16 17 **2. Cellular drug distribution**

18
19 To investigate cellular distribution of the drugs using confocal fluorescence microscopy, M109
20 and MDA-MB-231 cells were first treated with DOX or SQ-DOX NPs at a concentration of 1
21 μM during 1 h (figure 2). The red fluorescence emission corresponds to the drugs. To better
22 appreciate the localization of DOX and SQ-DOX NPs in the different cellular compartments,
23 drug fluorescence images were merged with transmission microscopy images. As shown in the
24 first and the fourth columns, fluorescence emission was predominantly localized in the cell
25 nucleus in the case of DOX treatment for both M109 and MDA-MB-231 cells, whereas after
26 SQ-DOX NPs treatment, fluorescence emission was localized both in the cytoplasm and the
27 nucleus. Since a correlation has been previously established between nuclear uptake of DOX
28 and its cytotoxic effect (38,39), fluorescence emission intensity from the nucleus has been
29 evaluated (figure 3). As shown, there was no significant difference in terms of fluorescence
30 emission intensity in the nucleus between DOX and SQ-DOX NPs treatments for both cell
31 lines; (figure 3). Cells were then treated with 5 μM of DOX or SQ-DOX NPs for respectively
32 1 and 5h. In the case of DOX treatment, drug fluorescence emission was still predominantly
33 localized in the nucleus for both 1 and 5 μM treatments (figure 2). Moreover, the intensity of
34 fluorescence emission increased when compared to 1 μM treatment during 1h in both cell lines
35 (figure 3). In the case of SQ-DOX NPs treatment at 5 μM for 1 h, fluorescence emission was
36
37
38
39
40
41
42
43
44
45
46
47
48
49
50
51
52
53
54
55
56
57
58
59
60
61
62
63
64
65

1 still localized in both cytoplasm and nucleus as show in figure 2 (second and fifth columns)
2 with an increase of the intensity of fluorescence emission from the nucleus (figure 3). A similar
3
4 distribution was observed in the case of the treatment for 5 hours as shown in figure 2 (third
5 and 6th columns) with an increase in the intensity of fluorescence emission from the nucleus
6
7 compared to the treatment for 1 hour (figure 3).
8
9
10

11 **Investigation of DOX and SQ-DOX NPs cellular uptake and distribution by Raman** 12 **microspectroscopy** 13 14 15

16 Raman microspectroscopy was used to track DOX and SQ-DOX NPs at the subcellular level
17 (nucleus and cytoplasm) and to distinguish, at the molecular level, the two forms of the drug
18 and their effects on the cellular components. The Chemical structures of DOX, SQ, and SQ-
19 DOX were displayed in figure 4a, 4b and 4c respectively. Figure 4d shows their average Raman
20 spectra in solution. Raman spectrum of free DOX exhibited the main characteristic bands
21 originated from the conjugated aromatic chromophore of the drug (substituted rings A, B and
22 C) (25). Table II listed the frequencies and tentative Raman bands assignments of DOX (27).
23
24 The spectrum of SQ-DOX NPs was dominated by the molecular signature of DOX (Figure 4d).
25
26 The main changes in Raman signature of SQ-DOX NPs were associated to a decrease in the
27 intensity of the band at 1210 cm^{-1} and the presence of an additional band at 1669 cm^{-1} , which
28 was attributed to SQ. These changes are related to the chemical linkage between SQ and DOX.
29
30 The main band in the Raman spectrum of SQ at 1669 cm^{-1} was attributed to the symmetric
31 stretching of the six double bonds in the compound. The other bands located in the region 1250 -
32 1400 cm^{-1} were attributed to various skeletal stretching and bending modes (CH_2/CH_3 bending,
33 $\omega(\text{CH})$ wag (in-plane), and $\gamma(\text{C-C})$ stretching) (40).
34
35
36
37
38
39
40
41
42
43
44
45
46
47
48
49
50
51
52
53

54 Raman microspectroscopy was first used to investigate the effects of both DOX and SQ-DOX
55 NPs at two concentrations (1 and $5\text{ }\mu\text{M}$) on the components in the cytoplasm and the nucleus
56 of M109 living single cell after 1 h treatment (Figure 5). The average spectra were shown with
57
58
59
60
61
62
63
64
65

1 their spectral variability. The spectra of untreated cells displayed common Raman bands
2 associated to proteins and/or lipids, and nucleic acids (Figure 5A). Band assignments of Raman
3 spectra of human cell lines are presented in Table 2. Cells were then treated with DOX and SQ-
4 DOX NPs, and difference spectra were calculated by subtracting mean Raman spectra measured
5 in the nucleus of control untreated cells from spectra measured in the nucleus of treated cells,
6 to better understand the effects of DOX and SQ-DOX NPs on the cellular components. These
7 difference spectra (b-a and c-a) revealed positive peaks that gave an estimation of the molecular
8 species highlighted in treated cells as compared to the control ones. These difference spectra
9 were superimposed with Raman spectrum of DOX in solution (Figure 5A). The difference in
10 spectrum (b-a) did not allow the identification of DOX features due to the low concentration
11 of DOX treatment at 1 μM . However, negative peaks observed in the difference spectrum at
12 frequencies of 782 cm^{-1} (O–P–O stretching mode of DNA backbone), 1100 (PO_2^- stretching
13 mode of the DNA), 1372 cm^{-1} (thymine), 1484, and 1575 cm^{-1} (adenine and guanine) were
14 assigned to nucleic acids content. These data are in agreement with the expected changes in
15 nucleus, probably related to the mechanism of action of the drug. However, at 5 μM , the
16 difference spectrum (c-a) showed positive bands at 1084, 1210, 1241, 1302, and 1443 cm^{-1}
17 associated to DOX features (Figure 5A). DOX bands at 1210, 1241 cm^{-1} were used as marker
18 of its uptake in the nucleus. The intensity of 1210/1241 cm^{-1} ratio related to DOX in the nucleus
19 decreased compared to free DOX, indicating intercalation of DOX in DNA. In addition, bands
20 1003, 1451 and 1661 cm^{-1} displayed were attributed to protein. The band at 1451 cm^{-1}
21 corresponds to the contribution of both CH_2 deformation mode arising from proteins and DOX
22 peak. These data suggested that the increase in the concentration of DOX, from 1 to 5 μM ,
23 resulted in a higher accumulation of nuclear DOX.

24 We then investigated the effects and the cellular distribution of SQ-DOX NPs in M109 cells
25 Figure 5B shows Raman spectra from nucleus of untreated and treated cells with SQ-DOX NPs.

1
2
3
4
5
6
7
8
9
10
11
12
13
14
15
16
17
18
19
20
21
22
23
24
25
26
27
28
29
30
31
32
33
34
35
36
37
38
39
40
41
42
43
44
45
46
47
48
49
50
51
52
53
54
55
56
57
58
59
60
61
62
63
64
65

These spectra exhibited Raman bands similar to those observed and attributed in Figure 5A. In the difference spectrum (b-a) (Figure 5B), which corresponded to 1 μM SQ-DOX NPs treatment, we have identified the two SQ-DOX bands at 1210 and 1241 cm^{-1} . The intensity of these two bands ratio was lower than for DOX. And as mentioned before, it is interesting to note that no detectable Raman signal was observed after DOX treatment at 1 μM (Figure 5A, b-a). No real changes in protein content were highlighted between untreated and SQ-DOX NPs treated cells. Unlike DOX, SQ-DOX NPs treatment did not induce any decrease in the nucleic acids content. However, by increasing the concentration of SQ-DOX NPs to 5 μM , difference spectrum (c-a, Figure 5B) was marked by very high Raman intensity of bands corresponding to DOX features. In addition, the intensity of 1210/1241 cm^{-1} ratio in difference spectrum (c-a) decreased as compared to (b-a) (Figure 5B). Such decrease suggests that released DOX is intercalated in DNA after hydrolysis.

We then investigated the distribution and the interaction of DOX and SQ-DOX NPs in the cytoplasm of M109 treated cells. Figure 6A and 6B, showed mean Raman spectra of the cytoplasm from untreated and treated cells after 1 h exposure time to either DOX or SQ-DOX NPs. Raman spectra measured in the cytoplasm of cells treated with 1 μM DOX were similar to those of control cells (Figure 6A). Difference spectra (Figure 6A, b-a and c-a) suggested that there were no evident DOX features in the cytoplasm, meaning that DOX was predominantly accumulated in the nucleus. In addition, DOX treatment did not induce significant changes in the proteins and lipids cytoplasmic contents. Difference spectra were then calculated for SQ-DOX NPs treatment and analyzed (Figure 6B, b-a, c-a). At 1 μM SQ-DOX NPs, the profile of the difference spectrum (b-a) was similar to that observed in the case of DOX treatment. When the cells were treated with 5 μM SQ-DOX, the drug was detected in the cytoplasm (Figure 7B, b-a).

1 Multivariate statistical analysis (PCA) was performed on two different datasets containing all
2 Raman images obtained from untreated and treated cells with DOX and SQ-DOX treatments at
3
4 concentration of 5 μM for 1 and 5 hours. PCA is used to investigate in more detail the
5
6 subcellular localization of these drugs. Six PCs, representing 95% of total variance in original
7
8 data were selected. Among these components, we have identified two PCs composed of the
9
10 bands at 1084, 1215, 1243, and 1445 cm^{-1} that could be attributed to the main characteristic
11
12 bands of DOX. Figure 8 showed these two DOX PCs spectra extracted respectively from the
13
14 two datasets, PC-Data1 for DOX and PC-Data2 for SQ-DOX NPs treatments. In order to better
15
16 visualize these peaks, Raman spectra of DOX and SQ-DOX in aqueous solutions were
17
18 displayed in the same figure. The intensity ratio 1215/1243 cm^{-1} in the spectra related to PC-
19
20 Data1 and PC-Data2 were comparable to those of free DOX and SQ-DOX respectively. Pseudo-
21
22 color scores images associated to these two PCs were reconstructed (Figure 9). White color
23
24 represents the area where no cellular information was present. Significant differences in the
25
26 localization of DOX and SQ-DOX NPs can be observed in the subcellular regions. In fact, for
27
28 both cell lines, the analysis PC-Data1 pseudocolor map showed that the scores related to this
29
30 component was very low in the cytoplasm and increased in the nucleus meaning that DOX was
31
32 only localized in the nucleus. The scores increased with the increase of the concentration of
33
34 DOX treatment. However, when the cells were incubated with SQ-DOX NPs at concentration
35
36 of 5 μM for 1h, PC-Data2 showed the distribution of the drug in the cytoplasm and the nucleus.
37
38 In fact, the scores maps showed that the drug was localized into cell cytoplasm and nucleus for
39
40 both cell lines. In addition, PC-Data2 scores were more intense in both two cell lines than those
41
42 of PC-Data1 meaning that SQ-Dox NPs accumulation was higher than DOX. When the cells
43
44 were treated with 5 μM of SQ-DOX NPs for 5h, PC-Data2 scores showed an increase in the
45
46 accumulation of the drug mainly in the nucleus. These data were in agreement with those
47
48 obtained using single point measurements on M109 cell line.
49
50
51
52
53
54
55
56
57
58
59
60
61
62
63
64
65

DISCUSSION

1
2
3 One of the most innovative and recent strategies in nanomedicine was the recent introduction
4
5 of the "squalenoylation" technology. Such strategy has allowed the emergence of new
6
7 treatments in cancer (41), neurological disorders (42), pain (43) and inflammation (44). The
8
9 "squalenoylation" method, initially developed with highly hydrophilic nucleosidic analogues
10
11 such as the gemcitabine (45–52) has been further extended to more hydrophobic drugs such as
12
13 paclitaxel(53) or doxorubicin (DOX) (16). In the case of DOX, conjugates were obtained by
14
15 the covalent linkage of SQ to DOX on the hydroxyl group of 14-C carbon atom (SQ-DOX)
16
17 allowing the formation of elongated SQ-DOX NPs in water, with a diameter of ~ 130 nm and
18
19 high drug loading (~ 57%) (16,54).
20
21
22
23
24

25 As shown in figure 1 and table 1, DOX was more cytotoxic than SQ-DOX NPs in M109 cells
26
27 *in vitro*. In fact, the IC₅₀ values of DOX were 7- and 10-times lower than the values
28
29 corresponding to SQ-DOX under long- and short-term treatment respectively. These data are
30
31 in agreement with those published earlier on MiaPaCa2 pancreatic carcinoma cells, which
32
33 suggested that this differential effect was due to the fact that the drug needs to be released to be
34
35 active (16). To investigate whether such cytotoxic effect was associated to an apoptotic effect,
36
37 annexin V staining and caspase-3/7 activity were evaluated. Both DOX and SQ-DOX NPs were
38
39 able to induce apoptosis (Figure 1c and d). As expected, DOX displayed a higher level of
40
41 apoptosis markers than SQ-DOX NPs. Altogether, cytotoxic and apoptotic data suggest that *in*
42
43 *vitro*, DOX is more active than SQ-DOX NPs. However, it is important to note that the main
44
45 advantage of SQ-DOX NPs lies in their efficacy *in vivo* where a reduction of blood clearance
46
47 and urinary excretion was observed together with higher tumor concentration of the drug (16).
48
49
50
51
52
53

54
55 As the aim was to investigate the incorporation and the cellular distribution of DOX and SQ-
56
57 DOX NPs, we first analyzed such parameters using confocal fluorescence microscopy. As
58
59 shown in figures 2 and 3, DOX accumulated predominantly in the cell nucleus. The fact that
60
61
62
63
64
65

1 the fluorescence emission remained relatively low resulted from the quenching of the
2 fluorescence emission upon intercalation of DOX in DNA(39). Similarly, a drug fluorescence
3 emission was also observed in the nucleus after treatment with SQ-DOX NPs. At the opposite
4 of DOX treatment, drug fluorescence emission was also observed in the cytoplasm, suggesting
5 that the hydrolysis of SQ-DOX NPs was necessary before the diffusion of DOX into the
6 nucleus. At this stage, confocal fluorescence microscopy analysis did not allow to distinguish
7 between DOX and SQ-DOX NPs in the different cellular compartments. On the other hand,
8 previous quantitative studies have provided evidence that the nuclear uptake of DOX correlated
9 with its cytotoxic effect (39). In order to characterize the different forms of the drugs at the
10 molecular level, particularly in the case of SQ-DOX NPs treatment, we subsequently analyzed
11 their cellular distribution by Raman microspectroscopy.

12 Raman microspectroscopy allowed the analysis of the cellular drug distribution and the cellular
13 biochemical changes upon treatment with DOX and SQ-DOX NPs. At a concentration of 5 μM ,
14 the intensity of Raman bands of DOX in the nucleus at 1210, 1241 cm^{-1} clearly appeared in the
15 difference spectrum between treated and untreated cells, indicating nuclear incorporation of the
16 drug (Figure 5). Moreover, the intensity of 1210/1241 cm^{-1} ratio decreased compared to DOX
17 in solution, suggesting the intercalation of DOX in DNA. We have previously reported that this
18 intercalation of DOX between base pairs of DNA was characterized by other changes related
19 to the decrease in the intensities of the bands at 1226 cm^{-1} , and 1255 cm^{-1} , and at 1461 cm^{-1}
20 (25). In addition, DOX treated cells exhibited a decrease in nucleic acid content which is
21 consistent with its mechanism of action, related to DNA synthesis inhibition (56, 57). Such
22 mechanisms include the inhibition of topoisomerase II activity upon its binding to DNA in a
23 ternary complex (56). This latter is consequently able to inhibit DNA replication. In addition,
24 the effect of DOX treatment was associated with an increase in the proteins content, which was
25 in agreement with data reported earlier (57).

1 After 1 μM treatment, data showed that Raman bands intensities attributed mainly to DOX were
2 higher in the cell nuclei after SQ-DOX NPs treatment when compared to DOX. Moreover, these
3 bands were observed only in the cytoplasm of cells treated with SQ-DOX NPs. When cells were
4 treated with 5 μM SQ-DOX, the intensities of these Raman bands increased markedly both in
5 the cytoplasm and the nucleus. In addition, the intensity of the 1210/1244 cm^{-1} ratio decreased
6 when compared to the treatment at a concentration of 1 μM , suggesting that a fraction of
7 hydrolyzed SQ-DOX was intercalated between base pairs of DNA. Unlike DOX, SQ-DOX NPs
8 treatment did not induce detectable decrease in the nucleic acids contents, which is in agreement
9 with the lowest cytotoxicity and apoptosis data.
10

11 Maksimenko *et al.* described that the internalization of SQ-DOX into the cells occurred via
12 endocytosis. The intracellular release of DOX from SQ-DOX NPs results from the hydrolysis
13 of the prodrug in lysosomes by esterases as reported earlier (16). The released drug is then
14 incorporated into the nucleus, allowing the induction of its biological effects. Our data clearly
15 show the presence of SQ in the cytoplasm, as it was expected. In fact, the band at 1669 cm^{-1} ,
16 which is specific to SQ, was observed in the difference spectrum recorded from the cytoplasm
17 of cells treated with SQ-DOX NPs and non-treated ones (Figure 6B). Interestingly, this band
18 was also detected in the nucleus of M109 cells treated with SQ-DOX NPs, suggesting that the
19 bioconjugate was probably able to diffuse into the nucleus (Figure 5B). We then asked whether
20 this observation could help to understand the discrepancy between the drug fluorescence
21 emission data observed in the nucleus and its biological effects. We thus analyzed the
22 interaction of SQ-DOX molecules with DNA in solution using surface enhanced Raman
23 scattering (SERS) to verify if SQ-DOX was able (or not) to intercalate into the DNA. SERS
24 spectra of SQ-DOX alone and in the presence of DNA with various ratios were measured. As
25 shown in supplementary Figure S1 and at the opposite of DOX, the comparison between spectra
26 of SQ-DOX, free and complexed to DNA at different molar ratio, did not show any changes in
27

1 the markers of DNA intercalation.. In other words, DNA intercalation should only occur in the
2 case of released DOX after SQ-DOX hydrolysis. This finding could explain the lower cytotoxicity
3 and apoptosis effects in the case of SQ-DOX NPs treatment. In fact, the Raman signal of the
4 drug in the nucleus (Figure 5 and 8) could be a combination of DOX and SQ-DOX spectral
5 features but only the fraction of DOX released from SQ-DOX could intercalate into the DNA
6 (Figure 5B), as confirmed in part by the relative decrease in the intensity 1210/1244 cm^{-1} ratio
7 (Figure 5B and 8). After 5 h treatment with SQ-DOX at 5 μM , the Raman spectral features
8 showed a higher 1210/1244 cm^{-1} ratio in the nucleus, suggesting a lowest fraction of the
9 intercalated form of DOX and a higher fraction of the non-hydrolyzed form of SQ-DOX (Figure
10 7a).

24 CONCLUSION

27 This study demonstrated the potential of Raman spectroscopy as a label free technique for the
28 *in vitro* characterization of the chemotherapeutic agents and their prodrug forms in single living
29 cancer cell. Our data provided simultaneous information on the detection of the different forms
30 of DOX and SQ-DOX NPs, and the identification of biochemical changes. Distinct Raman
31 spectroscopic markers of these chemotherapeutic agents were identified and used to understand
32 the mechanisms involved in the efficacy of the drugs *in vitro*. In conclusion, this study brings
33 new insights to the cellular characterization of anticancer drugs at the molecular level,
34 particularly in the field of nanomedicine.

49 ACKNOWLEDGEMENTS

51 The authors would like to thank the Platform of Cellular and Tissular Imaging (PICT) for
52 the equipment availability.

AUTHOR CONTRIBUTIONS

1
2 PC, HM and AB: Conception and design; FD, BS, AA, MC and AM: synthesis and
3
4 characterization of nanoparticles SQ-DOX; HR, LVG, AA, and AB: Methodology and data
5
6 acquisition ; HR, AA, HM and AB: Data analysis and manuscript writing; SM, DD, and PC:
7
8 Discussion and revision.
9

10
11
12 **Disclosure Statement:** PC is the founder of Squal Pharma, a start-up dedicated to the
13
14 development of squalenoylated nanomedicines. All other authors have nothing to disclose.
15
16

17
18 **Availability of data and materials:** All data generated or analyzed during this study are
19
20 included in this published article [and its supplementary information files]. If not, they are
21
22 available from the corresponding author on reasonable request.
23
24

25
26 **Funding:** This research did not receive any specific grant from funding agencies in the public,
27
28 commercial, or not-for-profit sectors.
29
30

REFERENCES

- 31
32
33
34
35
36 1. Higgins GS, O’Cathail SM, Muschel RJ, McKenna WG. Drug radiotherapy combinations:
37
38 review of previous failures and reasons for future optimism. *Cancer Treat Rev.* 2015
39
40 Feb;41(2):105–13.
41
42
43 2. Tacar O, Sriamornsak P, Dass CR. Doxorubicin: an update on anticancer molecular action,
44
45 toxicity and novel drug delivery systems. *J Pharm Pharmacol.* 2013 Feb;65(2):157–70.
46
47
48 3. Arcamone F. Properties of antitumor anthracyclines and new developments in their
49
50 application: Cain memorial award lecture. *Cancer Res.* 1985 Dec;45(12 Pt 1):5995–9.
51
52
53 4. Meredith A-M, Dass CR. Increasing role of the cancer chemotherapeutic doxorubicin in
54
55 cellular metabolism. *J Pharm Pharmacol.* 2016 Jun;68(6):729–41.
56
57
58
59
60
61
62
63
64
65

- 1
2
3
4
5
6
7
8
9
10
11
12
13
14
15
16
17
18
19
20
21
22
23
24
25
26
27
28
29
30
31
32
33
34
35
36
37
38
39
40
41
42
43
44
45
46
47
48
49
50
51
52
53
54
55
56
57
58
59
60
61
62
63
64
65
5. Thorn CF, Oshiro C, Marsh S, Hernandez-Boussard T, McLeod H, Klein TE, et al. Doxorubicin pathways: pharmacodynamics and adverse effects. *Pharmacogenetics and Genomics*. 2011 Jul;21(7):440–6.
6. Yang F, Teves SS, Kemp CJ, Henikoff S. Doxorubicin, DNA torsion, and chromatin dynamics. *Biochimica et Biophysica Acta (BBA) - Reviews on Cancer*. 2014 Jan;1845(1):84–9.
7. Pommier Y, Leo E, Zhang H, Marchand C. DNA Topoisomerases and Their Poisoning by Anticancer and Antibacterial Drugs. *Chemistry & Biology*. 2010 May;17(5):421–33.
8. Tan HH, Porter AG. DNA methyltransferase I is a mediator of doxorubicin-induced genotoxicity in human cancer cells. *Biochemical and Biophysical Research Communications*. 2009 May;382(2):462–7.
9. Yokochi T. Doxorubicin Inhibits DNMT1, Resulting in Conditional Apoptosis. *Molecular Pharmacology*. 2004 Aug 31;66(6):1415–20.
10. Carvalho C, Santos R, Cardoso S, Correia S, Oliveira P, Santos M, et al. Doxorubicin: The Good, the Bad and the Ugly Effect. *Current Medicinal Chemistry*. 2009 Sep 1;16(25):3267–85.
11. Octavia Y, Tocchetti CG, Gabrielson KL, Janssens S, Crijns HJ, Moens AL. Doxorubicin-induced cardiomyopathy: From molecular mechanisms to therapeutic strategies. *Journal of Molecular and Cellular Cardiology*. 2012 Jun;52(6):1213–25.
12. Brigger I, Dubernet C, Couvreur P. Nanoparticles in cancer therapy and diagnosis. *Advanced Drug Delivery Reviews*. 2002 Sep;54(5):631–51.
13. Cho K, Wang X, Nie S, Chen Z, Shin DM. Therapeutic Nanoparticles for Drug Delivery in Cancer. *Clinical Cancer Research*. 2008 Mar 1;14(5):1310–6.

14. Horcajada P, Chalati T, Serre C, Gillet B, Sebrie C, Baati T, et al. Porous metal–organic-framework nanoscale carriers as a potential platform for drug delivery and imaging. *Nature Materials*. 2010 Feb;9(2):172–8.
15. Shi J, Kantoff PW, Wooster R, Farokhzad OC. Cancer nanomedicine: progress, challenges and opportunities. *Nature Reviews Cancer*. 2016 Nov 11;17(1):20–37.
16. Maksimenko A, Dosio F, Mougín J, Ferrero A, Wack S, Reddy LH, et al. A unique squalenoylated and nonpegylated doxorubicin nanomedicine with systemic long-circulating properties and anticancer activity. *Proc Natl Acad Sci USA*. 2014 Jan 14;111(2):E217-226.
17. Bae YH, Park K. Targeted drug delivery to tumors: myths, reality and possibility. *J Control Release*. 2011 Aug 10;153(3):198–205.
18. Mallidis C, Sanchez V, Wistuba J, Wuebbeling F, Burger M, Fallnich C, et al. Raman microspectroscopy: shining a new light on reproductive medicine. *Hum Reprod Update*. 2014 Jun;20(3):403–14.
19. Neugebauer U, Rösch P, Popp J. Raman spectroscopy towards clinical application: drug monitoring and pathogen identification. *International Journal of Antimicrobial Agents*. 2015 Dec;46:S35–9.
20. Gala de Pablo J, Armistead FJ, Peyman SA, Bonthron D, Lones M, Smith S, et al. Biochemical fingerprint of colorectal cancer cell lines using label-free live single-cell Raman spectroscopy. *Journal of Raman Spectroscopy*. 2018 Aug;49(8):1323–32.
21. Guo J, Cai W, Du B, Qian M, Sun Z. Raman spectroscopic investigation on the interaction of malignant hepatocytes with doxorubicin. *Biophysical Chemistry*. 2009 Mar;140(1–3):57–61.

22. Schie IW, Alber L, Gryshuk AL, Chan JW. Investigating drug induced changes in single, living lymphocytes based on Raman micro-spectroscopy. *The Analyst*. 2014;139(11):2726–33.
23. Short KW, Carpenter S, Freyer JP, Mourant JR. Raman Spectroscopy Detects Biochemical Changes Due to Proliferation in Mammalian Cell Cultures. *Biophys J*. 2005 Jun;88(6):4274–88.
24. Swain RJ, Stevens MM. Raman microspectroscopy for non-invasive biochemical analysis of single cells. *Biochem Soc Trans*. 2007 Jun;35(Pt 3):544–9.
25. Beljebbar A, Sockalingum GD, Angiboust JF, Manfait M. Comparative FT SERS, resonance Raman and SERRS studies of doxorubicin and its complex with DNA. *Spectrochimica Acta Part A: Molecular and Biomolecular Spectroscopy*. 1995 Nov;51(12):2083–90.
26. Byrne HJ, Bonnier F, Casey A, Maher M, McIntyre J, Efeoglu E, et al. Advancing Raman microspectroscopy for cellular and subcellular analysis: towards in vitro high-content spectralomic analysis. *Appl Opt*. 2018 Aug 1;57(22):E11–9.
27. Das G, Nicastrì A, Coluccio ML, Gentile F, Candeloro P, Cojoc G, et al. FT-IR, Raman, RRS measurements and DFT calculation for doxorubicin. *Microscopy Research and Technique*. 2010;NA-NA.
28. Farhane Z, Bonnier F, Byrne HJ. An in vitro study of the interaction of the chemotherapeutic drug Actinomycin D with lung cancer cell lines using Raman micro-spectroscopy. *J Biophotonics*. 2018 Jan;11(1).
29. Farhane Z, Bonnier F, Howe O, Casey A, Byrne HJ. Doxorubicin kinetics and effects on lung cancer cell lines using in vitro Raman micro-spectroscopy: binding signatures, drug resistance and DNA repair. *J Biophotonics*. 2018 Jan;11(1).

- 1
2
3
4
5
6
7
8
9
10
11
12
13
14
15
16
17
18
19
20
21
22
23
24
25
26
27
28
29
30
31
32
33
34
35
36
37
38
39
40
41
42
43
44
45
46
47
48
49
50
51
52
53
54
55
56
57
58
59
60
61
62
63
64
65
30. Manfait M, Alix AJ, Jeannesson P, Jardillier JC, Theophanides T. Interaction of adriamycin with DNA as studied by resonance Raman spectroscopy. *Nucleic Acids Res.* 1982 Jun 25;10(12):3803–16.
 31. Moritz TJ, Taylor DS, Krol DM, Fritch J, Chan JW. Detection of doxorubicin-induced apoptosis of leukemic T-lymphocytes by laser tweezers Raman spectroscopy. *Biomedical Optics Express.* 2010 Nov 1;1(4):1138.
 32. Lê LMM, Berge M, Tfayli A, Zhou J, Prognon P, Baillet-Guffroy A, et al. Rapid discrimination and quantification analysis of five antineoplastic drugs in aqueous solutions using Raman spectroscopy. *European Journal of Pharmaceutical Sciences.* 2018 Jan;111:158–66.
 33. Birech Z, Mwangi PW, Bukachi F, Mandela KM. Application of Raman spectroscopy in type 2 diabetes screening in blood using leucine and isoleucine amino-acids as biomarkers and in comparative anti-diabetic drugs efficacy studies. *PLoS ONE.* 2017;12(9):e0185130.
 34. Bourget P, Amin A, Vidal F, Merlette C, Troude P, Baillet-Guffroy A. The contribution of Raman spectroscopy to the analytical quality control of cytotoxic drugs in a hospital environment: eliminating the exposure risks for staff members and their work environment. *Int J Pharm.* 2014 Aug 15;470(1–2):70–6.
 35. Nawaz H, Bonnier F, Knief P, Howe O, Lyng FM, Meade AD, et al. Evaluation of the potential of Raman microspectroscopy for prediction of chemotherapeutic response to cisplatin in lung adenocarcinoma. *The Analyst.* 2010;135(12):3070.
 36. Wolthuis R, Bakker Schut TC, Caspers PJ, Buschman HPJ, Romer TJ, Bruining HA, et al. In *Fluorescent and Luminescent Probes for Biological Activity.* Mason, WT, Ed. 1999;433–55.

- 1
2
3
4
5
6
7
8
9
10
11
12
13
14
15
16
17
18
19
20
21
22
23
24
25
26
27
28
29
30
31
32
33
34
35
36
37
38
39
40
41
42
43
44
45
46
47
48
49
50
51
52
53
54
55
56
57
58
59
60
61
62
63
64
65
37. Barnes RJ, Dhanoa MS, Lister SJ. Standard Normal Variate Transformation and Detrending of Near-Infrared Diffuse Reflectance Spectra. *Appl Spectrosc*, AS. 1989 May 1;43(5):772–7.
 38. Gigli M, Rasoanaivo TW, Millot JM, Jeannesson P, Rizzo V, Jardillier JC, et al. Correlation between growth inhibition and intranuclear doxorubicin and 4'-deoxy-4'-iododoxorubicin quantitated in living K562 cells by microspectrofluorometry. *Cancer Res*. 1989 Feb 1;49(3):560–4.
 39. Morjani H, Millot JM, Belhoussine R, Sebille S, Manfait M. Anthracycline subcellular distribution in human leukemic cells by microspectrofluorometry: factors contributing to drug-induced cell death and reversal of multidrug resistance. *Leukemia*. 1997 Jul;11(7):1170–9.
 40. Chun HJ, Weiss TL, Devarenne TP, Laane J. Vibrational spectra and DFT calculations of squalene. *Journal of Molecular Structure*. 2013 Jan;1032:203–6.
 41. Kotelevets L, Chastre E, Caron J, Mouglin J, Bastian G, Pineau A, et al. A Squalene-Based Nanomedicine for Oral Treatment of Colon Cancer. *Cancer Research*. 2017 Jun 1;77(11):2964–75.
 42. Gaudin A, Yemisci M, Eroglu H, Lepetre-Mouelhi S, Turkoglu OF, Dönmez-Demir B, et al. Squalenoyl adenosine nanoparticles provide neuroprotection after stroke and spinal cord injury. *Nature Nanotechnology*. 2014 Dec;9(12):1054–62.
 43. Feng J, Lepetre-Mouelhi S, Gautier A, Mura S, Cailleau C, Coudore F, et al. A new painkiller nanomedicine to bypass the blood-brain barrier and the use of morphine. *Science Advances*. 2019 Feb;5(2):eaau5148.
 44. Dormont F, Brusini R, Cailleau C, Reynaud F, Peramo A, Gendron A, et al. Squalene-based multidrug nanoparticles for improved mitigation of uncontrolled inflammation in rodents. *Science Advances*. 2020 Jun;6(23):eaaz5466.

- 1
2
3
4
5
6
7
8
9
10
11
12
13
14
15
16
17
18
19
20
21
22
23
24
25
26
27
28
29
30
31
32
33
34
35
36
37
38
39
40
41
42
43
44
45
46
47
48
49
50
51
52
53
54
55
56
57
58
59
60
61
62
63
64
65
45. Couvreur P, Stella B, Reddy LH, Hillaireau H, Dubernet C, Desmaële D, et al. Squalenoyl Nanomedicines as Potential Therapeutics. *Nano Letters*. 2006 Nov;6(11):2544–8.
 46. Desmaële D, Gref R, Couvreur P. Squalenoylation: A generic platform for nanoparticulate drug delivery. *Journal of Controlled Release*. 2012 Jul;161(2):609–18.
 47. Reddy LH, Renoir J-M, Marsaud V, Lepetre-Mouelhi S, Desmaële D, Couvreur P. Anticancer Efficacy of Squalenoyl Gemcitabine Nanomedicine on 60 Human Tumor Cell Panel and on Experimental Tumor. *Molecular Pharmaceutics*. 2009 Oct 5;6(5):1526–35.
 48. Reddy LH, Khoury H, Paci A, Deroussent A, Ferreira H, Dubernet C, et al. Squalenoylation Favorably Modifies the in Vivo Pharmacokinetics and Biodistribution of Gemcitabine in Mice. *Drug Metabolism and Disposition*. 2008 Aug;36(8):1570–7.
 49. Reddy LH, Marque P-E, Dubernet C, Mouelhi S-L, Desmaële D, Couvreur P. Preclinical Toxicology (Subacute and Acute) and Efficacy of a New Squalenoyl Gemcitabine Anticancer Nanomedicine. *Journal of Pharmacology and Experimental Therapeutics*. 2008 May;325(2):484–90.
 50. Reddy LH, Dubernet C, Mouelhi SL, Marque PE, Desmaele D, Couvreur P. A new nanomedicine of gemcitabine displays enhanced anticancer activity in sensitive and resistant leukemia types. *Journal of Controlled Release*. 2007 Dec;124(1–2):20–7.
 51. Sobot D, Mura S, Rouquette M, Vukosavljevic B, Cayre F, Buchy E, et al. Circulating Lipoproteins: A Trojan Horse Guiding Squalenoylated Drugs to LDL-Accumulating Cancer Cells. *Mol Ther*. 2017 05;25(7):1596–605.
 52. Sobot D, Mura S, Yesylevskyy SO, Dalbin L, Cayre F, Bort G, et al. Conjugation of squalene to gemcitabine as unique approach exploiting endogenous lipoproteins for drug delivery. *Nat Commun*. 2017 30;8:15678.
 53. Caron J, Maksimenko A, Wack S, Lepeltier E, Bourgaux C, Morvan E, et al. Improving the Antitumor Activity of Squalenoyl-Paclitaxel Conjugate Nanoassemblies by

1 Manipulating the Linker between Paclitaxel and Squalene. *Advanced Healthcare*
2 *Materials*. 2013 Jan;2(1):172–85.
3

- 4
5 54. Mougín J, Yesylevskyy SO, Bourgaux C, Chapron D, Michel J-P, Dosio F, et al. Stacking
6 as a Key Property for Creating Nanoparticles with Tunable Shape: The Case of
7 Squalenoyl-Doxorubicin. *ACS Nano*. 2019 Nov 26;13(11):12870–9.
8
9
10
11 55. Nawaz H, Garcia A, Meade AD, Lyng FM, Byrne HJ. Raman micro spectroscopy study
12 of the interaction of vincristine with A549 cells supported by expression analysis of bcl-2
13 protein. *Analyst*. 2013;138(20):6177.
14
15
16
17 56. Komiyama T, Oki T, Inui T. Interaction of new anthracycline antibiotics with DNA.
18 Effects on nucleic acid synthesis and binding to DNA. *Biochimica et Biophysica Acta*
19 (BBA) - Gene Structure and Expression. 1983 May 20;740(1):80–7.
20
21
22
23
24
25
26 57. Farhane Z, Bonnier F, Byrne HJ. Monitoring doxorubicin cellular uptake and trafficking
27 using in vitro Raman microspectroscopy: short and long time exposure effects on lung
28 cancer cell lines. *Analytical and Bioanalytical Chemistry*. 2017 Feb;409(5):1333–46.
29
30
31
32
33
34
35
36
37
38
39
40
41
42
43
44
45
46
47
48
49
50
51
52
53
54
55
56
57
58
59
60
61
62
63
64
65

Legend figure

Figure 1: Antitumor activity of DOX and SQ-DOX on M109 cell growth (a and b) and apoptosis (c and d). For cell growth inhibition, cells were treated with concentrations ranging from 0.1 nM to 1 μ M for a) 72h time exposure and b) 1h treatment and 72h post-incubation after washing. For apoptosis, flow cytometry analysis of (c) Annexin V and (d) Caspase 3/7 expressed by the percentage of M109 apoptotic positive cells assessed using the Muse Annexin V and Caspase 3/7 assay kit. Cell growth rate is expressed as percentage compared to untreated cells control; error bars indicating standard deviation of three duplicated independent measurements. For apoptosis, values represent the mean \pm SEM of three independent experiments (n=3, Mann & Whitney test).

Figure 2: Fluorescence microscopy images of M109 and MDA-MB-231 cells treated with DOX and SQ-DOX at concentrations of 1 μ M (1h) and 5 μ M (1 and 5hrs). These images showed the intracellular uptake of free DOX and SQ-DOX NPs (in red) and its merge with the bright field image of the corresponding cell (x63, scale bar = 10 μ m).

Figure 3: Quantification the nuclear accumulation of DOX and SQ-DOX at concentrations of 1 μ M and 5 μ M from the analysis of fluorescence images using ImageJ software. Regions-of-interest (ROIs) were selected on each cell nucleus (M109 and MDA-MB-231) treated with DOX and SQ-DOX NPs. The average fluorescence intensity was calculated for each drug at 1 h and 5 h exposition time.

Figure 4: Chemical structure of a) DOX, b) SQ, c) SQ-DOX, and d) their Raman spectra in solutions.

Figure 5: Mean Raman spectra measured on untreated cell nucleus (a) and nucleus treated for 1 h with DOX (panel A) and SQ-DOX (panel B) with concentrations of: b) 1 μ M, and c) 5 μ M. 10 spectra were measured on each cell nucleus with an acquisition time of 10 seconds in the fingerprint region 570-1800 cm^{-1} . The shaded areas represent the respective standard deviations. Difference spectra (b-a, c-a) were obtained by subtracting Raman spectra treated cell with concentration of 1 μ M and 5 μ M from untreated cells.

Figure 6: Mean Raman spectra measured on untreated cell cytoplasm (a) and cytoplasm treated for 1 h with DOX (panel A) and SQ-DOX (panel B) with concentrations of: b) 1 μ M, c) 5 μ M. 10 spectra were measured on each cell cytoplasm with an acquisition time of 10 seconds in the fingerprint region 570-1800 cm^{-1} . The shaded areas represent the respective standard deviations. Difference spectra (b-a, c-a) were obtained by subtracting Raman spectra treated cell with concentration of 1 μ M and 5 μ M from untreated cells.

Figure 7: Mean Raman spectra measured on nucleus (panel A) and cytoplasm (pane B) on untreated cell (a) and treated 5 h with SQ-DOX at concentration of 5 μ M (b). Difference spectra (b-a) was obtained by subtracting Raman spectra treated cell with concentration of 5 μ M from untreated cells. The shaded areas represent the respective standard deviations.

Figure 8: Comparison between the two PCs (PC-Data1 and PC-Data2) potentially attributed to DOX or SQ-DOX and Raman spectra of DOX and SQ-DOX in aqueous solutions.

Figure 9: Pseudo-color scores images associated to PC-Data1 and PC-Data2 from M109 and MDA-MB-231 cells treated with DOX and SQ-DOX treatments at concentration of 5 μ M for

1 and 5 hours. These maps displayed significant differences in the localization of these drugs in the subcellular regions.

1
2
3
4
5
6
7
8
9
10
11
12
13
14
15
16
17
18
19
20
21
22
23
24
25
26
27
28
29
30
31
32
33
34
35
36
37
38
39
40
41
42
43
44
45
46
47
48
49
50
51
52
53
54
55
56
57
58
59
60
61
62
63
64
65

**Investigation of squalene-doxorubicin distribution and interactions within single living
cancer cell using Raman microspectroscopy**

H. Rammal^{1, ¶}, F. Dosio², B. Stella², A. Maksimenko³, S. Mura³, L. Van Gulick¹, A. Al
Assaad¹, D. Desmaële³, P. Couvreur³, H. Morjani^{1#}, A. Beljebbar^{1#*}

1. Translational BioSpectroscopy, BioSpecT, EA 7506, Université de Reims, Faculté de Pharmacie, Reims, France
2. Department of Drug Science and Technology, University of Torino, 10125 Torino, Italy
3. Institut Galien Paris-Saclay CNRS UMR8612, Université Paris-Saclay, Faculté de Pharmacie, Châtenay-Malabry, France.

[#]H M and A B co-supervised this work

[¶]Present address : EFOR Healthcare Paris, Biocompatibility Platform, 92300 Levallois-Perret, France.

***: Correspondence should be sent to:**

Dr. Abdelilah BELJEBBAR
Translational BioSpectroscopy, EA 7506
UFR de Pharmacie
Université de Reims Champagne-Ardenne
51, rue Cognacq-Jay,
51096 Reims CEDEX, France
Phone: (33) 3 2691-8376
Fax: (33) 3 2691-8282
E-mail: abdelilah.beljebbar@univ-reims.fr

ABSTRACT

1
2 Intracellular distribution of doxorubicin (DOX) and its squalenoylated (SQ-DOX)
3
4 nanoparticle (NP) form in living lung carcinoma M109 cells were investigated by Raman
5
6 microspectroscopy. Pharmacological data showed that DOX induced higher cytotoxic effect
7
8 than SQ-DOX NPs. Raman data showed that after DOX treatment at 1 μM , the spectral
9
10 features of DOX were not detected in the cell cytoplasm and nucleus. 5 μM treatment allowed
11
12 to detect in the nucleus the Raman bands of DOX at 1211 and 1241 cm^{-1} . Moreover, the
13
14 intensity ratio of these bands decreased, indicating DOX intercalation into DNA. However,
15
16 after treatment with SQ-DOX NPs, the intensity of these Raman bands increased.
17
18 Interestingly, with SQ-DOX NPs, the intensity of 1210/1241 cm^{-1} ratio was higher suggesting
19
20 a lower fraction of intercalated DOX in DNA and higher amount of non-hydrolyzed SQ-
21
22 DOX. These data could explain the lower cytotoxic effect of SQ-DOX NPs *in vitro*.
23
24
25
26
27
28
29
30

31 **Key words:** Raman microspectroscopy; living cancer cells, squalenoylated doxorubicin,
32
33 nanoparticles
34
35
36
37
38
39
40
41
42
43
44
45
46
47
48
49
50
51
52
53
54
55
56
57
58
59
60
61
62
63
64
65

Introduction

1
2 Cancer treatment is often limited by a lack of selectivity and toxicity(1,2). Doxorubicin
3
4 (DOX) emerged as one of the most widely used anti-cancer chemotherapeutic drug (3,4).
5
6 Generally, it is accepted that DOX has the ability to intercalate between the G-C base pairs
7
8 (5,6) and to inhibit DNA topoisomerase II resulting in inhibition of DNA replication and cell
9
10 growth (9–11). Unfortunately, the use of DOX in clinic encounters some limitations,
11
12 including a lack of selectivity, cardiotoxicity and development of resistance (5,12,13).
13
14

15
16 One of the used strategies to improve antitumor efficacy, tissue distribution and
17
18 pharmacokinetics of anticancer drugs is the development of nanoscale drug delivery systems
19
20 (*i.e.* nanomedicine) (14). In this context, various nanocarriers of DOX have been developed
21
22 (15–17). Recently, the chemical linkage of DOX to squalene (SQ), a natural lipid precursor of
23
24 the cholesterol's biosynthesis, has been proposed (18). Such bioconjugate (SQ-DOX) was
25
26 found to spontaneously self-assemble in water in form of nanoparticles (NPs) of 130-nm
27
28 mean diameter. *In vivo*, SQ-DOX NPs were found to reduce murine pancreatic tumor growth
29
30 by 95%, compared to only a 29% DOX. In M109 murine lung carcinoma, a 90% tumor
31
32 inhibition was observed SQ-DOX NPs, whereas DOX was ineffective. In addition, SQ-DOX
33
34 NPs were five-fold better tolerated than DOX, thus significantly reducing both cardiac and
35
36 digestive toxicities (18).
37
38

39
40 A better understanding of the mechanism behind the observed anticancer efficacy, including
41
42 cellular uptake, intracellular distribution and subcellular interactions is crucial to improve the
43
44 benefit/risk ratio of this approach. Interestingly, near infrared Raman microspectroscopy
45
46 emerged as an attractive label-free and a non-invasive methodology for monitoring the
47
48 molecular information associated with the biological activity of anticancer agents (19–21).
49
50 This technique has been previously used to analyze biochemical information simultaneously
51
52 on both the drug and the cell components (*i.e.* DNA, RNA, proteins, and lipid content) (22–
53
54
55
56
57
58
59
60
61
62
63
64
65

1 25). Additionally, Raman spectroscopy has the ability to study cells in physiological
2 conditions with high spatial resolution (26). Several studies have already investigated the
3 effect of DOX and its interaction with DNA at the molecular and cellular levels using Raman
4 spectroscopy (24,27–33). This technique was also used for preclinical applications such as the
5 quantification of antineoplastic drugs in the tumor (34), and the screening of early stage
6 cellular response to different drug treatments for improving drug efficacy and reducing
7 toxicity (34–37).
8

9
10
11
12
13
14
15
16
17 Herein, we shed light on the potential use of Raman microspectroscopy to investigate the
18 intracellular distribution and interaction of DOX and SQ-DOX NPs in cytoplasmic and
19 nuclear compartments of living murine lung carcinoma cell line (M109) *in vitro*.
20
21
22

23 **MATERIALS AND METHODS**

24 **1. Drugs**

25
26
27
28
29
30
31
32
33
34
35
36
37
38
39
40
41
42
43
44
45
46
47
48
49
50
51
52
53
54
55
56
57
58
59
60
61
62
63
64
65
DOX was purchased from Sigma-Aldrich (Saint-Quentin Fallavier, France). The chemical
structure of DOX consists of a tetracyclic ring with the sugar daunosamine attached by a
glycosidic linkage. SQ was purchased from Sigma-Aldrich. This molecule is a
polyunsaturated hydrocarbon of the triterpene type. SQ-DOX was synthesized by chemical
linkage of the anticancer drug DOX onto SQ (18). SQ-DOX NPs were prepared using the
nanoprecipitation method. Briefly, 500 μ L of a tetrahydrofuran solution of SQ-DOX (4
mg/mL) was added drop-wise under stirring (500 rpm) into 1 mL distilled water. Precipitation
of the SQ-DOX NPs occurred spontaneously after evaporation of tetrahydrofuran. The
diameter of the nanoparticles was determined by laser light scattering at 20 °C using a
nanosizer (Zetasizer Nano ZS, Malvern Instrument, UK).

66 **2. Cancer cell culture**

67
68
69
70
71
72
73
74
75
The murine lung carcinoma (M109) cell line was obtained from the American Type Culture
Collection (ATCC) and maintained as recommended. Briefly, cells were cultured in RPMI

1 medium 1640 (Gibco) supplemented with 10% heat-inactivated fetal bovine serum (FBS),
2 penicillin (100 U/mL) and streptomycin (100 µg/mL). Cells were kept in a humidified
3 atmosphere of 5% CO₂ with a medium change every two days and were routinely passaged at
4 pre-confluency using 0.05% trypsin, 0.53 mM EDTA (Invitrogen) and screened for the
5 absence of mycoplasma using PCR methods.
6
7
8
9

10 **3. Cytotoxicity assay**

11
12 5×10^4 cells in exponential growth phase were allowed to adhere on 24 well plate for 24 h at
13 37 °C in a humidified atmosphere of 5% CO₂ in air. After pre-incubation, M109 cells were
14 washed with sterile phosphates-buffered saline (PBS) and then exposed to series of
15 concentrations of free DOX or SQ-DOX NPs ranging from 0.1 nM to 1 µM for 72 h.
16 Untreated cells were used as control. For short time drug exposure, cells were exposed to
17 series of concentrations of free DOX or SQ-DOX ranging from 0.1 µM to 50 µM for 1 h.
18 After the short time incubation, the culture medium containing the drug was removed, cells
19 were then washed and incubated with a new culture medium for 72 h. Afterwards, in both
20 protocols, cells were then washed and detached using 0.05% trypsin, 0.53 mM EDTA and
21 counted using a traditional cell Kova[®] slide counting plate (Kova international). The
22 inhibitory concentration 50% (IC₅₀) was defined as the drug (DOX or SQ-DOX) concentration
23 required to inhibit M109 cell growth by 50%, relative to untreated controls. IC₅₀ values were
24 estimated from the dose response curves plotted using GraphPad Prism[®] 6 software and
25 provided from the average of three different experiments and in duplicate at each time.
26
27
28
29
30
31
32
33
34
35
36
37
38
39
40
41
42
43
44
45
46
47

48 **4. Annexin V and Caspase 3/7 analysis**

49
50 10^5 cells in exponential growth phase were allowed to adhere on six well plate for 24 h at 37
51 °C in a humidified atmosphere of 5% CO₂ in air. After pre-incubation, M109 cells were then
52 washed with sterile PBS and incubated for 48 h with free DOX or SQ-DOX NPs at the
53 concentration of 100 nM. After treatment, cells were harvested using trypsin-EDTA, washed
54
55
56
57
58
59
60
61
62
63
64
65

1 two times with PBS, and re-suspended in fresh culture medium containing 10 % serum. Cell
2 suspensions were stained using the Muse™ Annexin V and Caspase 3/7 kit (Millipore,
3 Molsheim, France) according to manufacturer's instructions. Data were acquired on a Muse™
4 Cell Analyzer (Millipore, Molsheim, France).
5
6
7

8 9 10 **5. Cellular drug distribution by confocal fluorescence microscopy**

11 M109 cells were cultured in an 8-well Nunc® Lab-Tek® II Chamber Slide™ system (Nunc),
12 to achieve 40–60% confluence after 24 h at 37 °C in a humidified atmosphere of 5% CO₂ in
13 air. Cells were then washed with sterile PBS and incubated for 1 h with free DOX or SQ-DOX
14 NPs at the concentration of 1 μM (37 °C). After treatment, unfixed cells were
15 washed/discarded and the remaining ones were stained for 10 min with 4 μg/mL nuclear DNA
16 fluorescent dye Hoechst 33342, trihydrochloride, trihydrate (Invitrogen, Illkirch, France) and
17 observed by fluorescence microscopy using incandescent tungsten-halogen lamps and
18 appropriate excitation and emission filters 350_{Ex}/460_{Em} and 488_{Ex}/560_{Em} for, Hoechst 33342
19 and DOX visualization, respectively (Zeiss microscopy, × 63 oil immersion objective).
20
21
22
23
24
25
26
27
28
29
30
31
32
33

34 **6. Cellular drug accumulation and confocal laser microspectrofluorometry**

35 The monitoring of the nuclear incorporation of DOX into the nucleus of cells was carried out
36 using the microspectrofluorimeter M51 (Horiba Jobin Yvon France, Villeneuve d'Ascq). Cells
37 were seeded in petri dish 24 h prior to the measurements. After treatment with DOX and SQ-
38 DOX NPs, cells were washed with PBS and placed in medium (free of drugs) without phenol
39 red. To obtain fluorescence emission spectra, the 488 nm line was used with an ionized Argon
40 laser (2065 series, SpectraPhysics, Les Ulis, France). A nuclear spectrum of treated cells was
41 obtained over the wavelength range 500-700 nm (39). The semi-quantification of the nuclear
42 incorporation of DOX was obtained by measuring the fluorescence emission intensity of the
43 band at the 690 nm wavelength.
44
45
46
47
48
49
50
51
52
53
54
55
56
57

58 **7. Raman microspectroscopy**

1 Raman spectra were recorded with a near infrared confocal Raman spectrometer (Labram
2 ARAMIS, Horiba Jobin Yvon S.A.S., France). This setup consisted of a microscope
3
4 (Olympus, BX41, France) coupled to the Raman spectrometer equipped with 600 groove/mm
5
6 diffraction grating. The microscope was equipped with a xy-motorized (Marzhauser,
7
8 Germany), computer-controlled sample stage, which enabled automatic scanning of the
9
10 sample with a spatial resolution of 1 μm . The excitation source (785 nm) was provided by
11
12 diode laser (Toptica Photonics, Germany) delivering 60 mW of laser power on the sample.
13
14 This laser excitation was focused on the single cell with water immersion NIR 100x objective
15
16 (NA 1.0, Olympus, France). This backscattered light was collected by the objective and was
17
18 transmitted to the spectrometer equipped with a Pelletier-cooled charge-coupled device
19
20 detector. Adherent M109 cells ($50 \cdot 10^3$ cells/mL /window) were seeded directly on previously
21
22 sterilized CaF_2 windows in 6-well plate 24 h before treatment. Cells were incubated with or
23
24 without DOX or SQ-DOX nanoparticles at concentrations of 1, 5, and 10 μM and placed into
25
26 petri dishes for 1 h and 5 h. After incubation, medium was then removed and cells were rinsed
27
28 twice with sterile PBS. Cells were kept in PBS for Raman acquisition. Spectra were acquired
29
30 on five different cells. For each cell, 15 measurements were performed at two different cell
31
32 compartments: nucleus and cytoplasm (figure 1), using a 20 seconds integration time in the
33
34 $600\text{--}1800\text{ cm}^{-1}$ spectral region with a spectral resolution of 4 cm^{-1} . Data acquisition was
35
36 carried out by means of the LabSpec 5 software (Horiba Jobin Yvon S.A.S. France).
37
38
39
40
41
42
43
44
45

46 **8. Data pretreatment**

47
48 Various data processing were performed to extract the tissue Raman signal from the raw
49
50 measured spectra (59). After acquisition, spectra were first calibrated using Raman calibration
51
52 standards. The spectrum of the halogen lamp was used to correct for the wavelength-
53
54 dependent signal detection efficiency of the Raman setup. Raman data were analyzed with
55
56 custom software developed in MatLab (MathWorks, Inc., Matick, USA). All spectra were
57
58
59
60
61
62
63
64
65

1 corrected for the PBS solution and Caf₂ background, baseline corrected using a fourth order
2 polynomial and smoothed with fifth points Savitzky-Golay algorithm in order to minimize the
3 influence of noises. The resulting spectra were then normalized using a Standard Normal
4 Variate (SNV) procedure (60).
5
6
7

8 9 **9. Statistical analysis**

10 ANOVA test was performed using GraphPad Prism 6 software. Statistical significance was
11 assessed by followed by Sidak simple comparison test (*p < 0.05, ***p < 0.001).
12
13
14
15

16 **RESULTS**

17 **Antitumor activity of DOX and SQ-DOX**

18
19 In order to evaluate DOX and SQ-DOX NPs antitumor activity, M109 cells were pre-
20 incubated for 24 h and then exposed to concentrations of DOX and SQ-DOX NPs ranging
21 from 0.1 nM to 1μM.. Dose-response assays plots allowed to calculate the drug concentration,
22 which induces 50% cell growth inhibition (IC₅₀). After long-term treatment, DOX and SQ-
23 DOX NPs inhibited the growth of M109 cells in a concentration-dependent manner and the
24 calculated IC₅₀ were respectively 2.6 and 18 nM (Figure 2a, table 1). After short-term
25 treatment, DOX and SQ-DOX NPs induced also a decrease in cell growth with IC₅₀ values of
26 0.12 and 1.2 μM, respectively (Figure 2b, table 1). To investigate the drug-induced apoptosis,
27 M109 cells were treated with DOX or SQ-DOX NPs at concentration of 100 nM. After 48 h
28 incubation, Annexin-V staining revealed that SQ-DOX treatment induced 45% apoptosis,
29 whereas DOX treatment induced 75% positive (Figure 2C) (p<0.001). These results were
30 concomitant with caspase 3/7 staining, a hallmark of the apoptosis induction, showing a
31 higher caspase 3/7 activation upon DOX treatment with 43% of positive cells compared to
32 only 30% upon SQ-DOX treatment (p<0.05) (Figure 2d). While *in vivo* SQ-DOX treatment
33 markedly inhibited M109 tumors (90% with SQ-DOX vs 3% with DOX) demonstrating the
34 efficacy of this nanomedicine even in a drug-resistant tumor model, the *in vitro* results failed
35
36
37
38
39
40
41
42
43
44
45
46
47
48
49
50
51
52
53
54
55
56
57
58
59
60
61
62
63
64
65

1 to highlight such effects (18). This inconsistency is rather usual in the nanomedicine field, due
2 to the slow release of the parent drug from SQ-DOX nanoparticles and to their improved
3 pharmacokinetic (*i.e.* reduced clearance), reduced elimination and tumor specific
4 biodistribution.
5
6
7
8

9 **Cellular drug distribution and nuclear uptake**

10 To investigate cellular uptake and distribution of the drug , M109 cells were treated with
11 DOX or SQ-DOX NPs at a concentration of 1 μ M during 1 h. Figure 3a and 3b displayed the
12 transmission microscopy of M109 treated cells. Confocal fluorescence microscopy was used
13 to follow intracellular distribution of DOX and SQ-DOX NPs. The blue fluorescence
14 emission corresponds to the nuclear DNA staining with Hoechst33342 (figure 3c and 3d),
15 while the red fluorescence emission corresponds to DOX or SQ-DOX NPs (figure 3e and 3f).
16 To better distinguish the location of DOX and SQ-DOX NPs in the different cellular
17 compartments, the merged images associating DNA staining and drug fluorescence emission
18 are shown in figure 3g and 3h. After 1 h treatment with DOX, the drug predominantly
19 accumulated in the cell nucleus, whereas after SQ-DOX NPs treatment fluorescence emission
20 was located both in the cytoplasm and the nucleus. Since a correlation has been established
21 between nuclear uptake of DOX and its cytotoxic effect (38,39), microspectrofluorometry was
22 used to quantify DOX or SQ-DOX NPs uptake (40). Cells were treated with DOX or SQ-
23 DOX NPs at a concentration of 1 μ M. After various incubation times, fluorescence emission
24 spectra were recorded from a microvolume of single living cell nuclei. As shown in figure 4,
25 the emission intensity was around 100 (a.u.) in the cell nuclei after 1 h of DOX treatment.
26 After 5 h treatment, the fluorescence emission intensity was 2-fold higher and was around 200
27 (a.u.). Remarkably, the emission intensity was higher after SQ-DOX NPs treatment (1 h) and
28 increased slowly over time to reach a value of 300 (a.u.) (figure 4).
29
30
31
32
33
34
35
36
37
38
39
40
41
42
43
44
45
46
47
48
49
50
51
52
53
54
55
56
57
58
59
60
61
62
63
64
65

Investigation of DOX and SQ-DOX NPs cellular uptake and distribution by Raman microspectroscopy

Raman microspectroscopy was used to track DOX and SQ-DOX NPs at the subcellular level (nucleus and cytoplasm) (Figure 1) and to distinguish, at the molecular level, the two forms of the drug and their effects on the cellular components. The Chemical structures of DOX, SQ, and SQ-DOX were displayed in figure 5a, 5b and 5c respectively. Figure 5d shows their average Raman spectra in solution. Raman spectrum of free DOX exhibited the main characteristic bands originated from the conjugated aromatic chromophore of the drug (substituted rings A, B and C) (27). Table II listed the frequencies and tentative Raman bands assignments of DOX (29). The spectrum of SQ-DOX NPs was dominated by the molecular signature of DOX (Figure 5d). The main changes in Raman signature of SQ-DOX NPs were associated to a decrease in the intensity of the band at 1210 cm^{-1} and the presence of an additional band at 1669 cm^{-1} , which was attributed to SQ. These changes are related to the chemical linkage between SQ and DOX. The main band in the Raman spectrum of SQ at 1669 cm^{-1} was attributed to the symmetric stretching of the six double bonds in the compound. The other bands located in the region $1250\text{-}1400\text{ cm}^{-1}$ were attributed to various skeletal stretching and bending modes (CH_2/CH_3 bending, $\omega(\text{CH})$ wag (in-plane), and $\gamma(\text{C-C})$ stretching) (41).

Raman microspectroscopy was first used to investigate the effects of both DOX and SQ-DOX NPs at two concentrations (1 and $5\text{ }\mu\text{M}$) on the components in the cytoplasm and the nucleus of M109 living single cell after 1 h treatment (Figure 6). The average spectra were shown with their spectral variability. The spectra of untreated cells displayed common Raman bands associated to proteins and/or lipids, and nucleic acids (Figure 6A). Band assignments of Raman spectra of human cell lines are presented in Table 2. Cells were then treated with DOX and SQ-DOX NPs, and difference spectra were calculated by subtracting mean Raman spectra

1 measured in the nucleus of control untreated cells from spectra measured in the nucleus of
2 treated cells, to better understand the effects of DOX and SQ-DOX NPs on the cellular
3 components. These difference spectra (b-a and c-a) revealed positive peaks that gave an
4 estimation of the molecular species highlighted in treated cells as compared to the control
5 ones. These difference spectra were superimposed with Raman spectrum of DOX in solution
6 (Figure 6A). The difference in spectrum (b-a) did not allow the identification of DOX
7 features due to the low concentration of DOX treatment at 1 μM . However, negative peaks
8 observed in the difference spectrum at frequencies of 782 cm^{-1} (O–P–O stretching mode of
9 DNA backbone), 1100 (PO^{2-} stretching mode of the DNA), 1372 cm^{-1} (thymine), 1484, and
10 1575 cm^{-1} (adenine and guanine) were assigned to nucleic acids content. These data are in
11 agreement with the expected changes in nucleus, probably related to the mechanism of action
12 of the drug. However, at 5 μM , the difference spectrum (c-a) showed positive bands at 1084,
13 1210, 1241, 1302, and 1443 cm^{-1} associated to DOX features (Figure 6A). DOX bands at
14 1210, 1241 cm^{-1} were used as marker of its uptake in the nucleus. The intensity of 1210/1241
15 cm^{-1} ratio related to DOX in the nucleus decreased compared to free DOX, indicating
16 intercalation of DOX in DNA. In addition, bands 1003, 1451 and 1661 cm^{-1} displayed were
17 attributed to protein. The band at 1451 cm^{-1} corresponds to the contribution of both CH_2
18 deformation mode arising from proteins and DOX peak. These data suggested that the
19 increase in the concentration of DOX, from 1 to 5 μM , resulted in a higher accumulation of
20 nuclear DOX.

21 We then investigated the effects and the cellular distribution of SQ-DOX NPs in M109 cells
22 Figure 6B shows Raman spectra from nucleus of untreated and treated cells with SQ-DOX
23 NPs. These spectra exhibited Raman bands similar to those observed and attributed in Figure
24 6A. In the difference spectrum (b-a) (Figure 6B), which corresponded to 1 μM SQ-DOX NPs
25 treatment, we have identified the two SQ-DOX bands at 1210 and 1241 cm^{-1} . The intensity of

1 these two bands ratio was lower than for DOX. And as mentioned before, it is interesting to
2 note that no detectable Raman signal was observed after DOX treatment at 1 μM (Figure 6A,
3 b-a). No real changes in protein content were highlighted between untreated and SQ-DOX
4 NPs treated cells. Unlike DOX, SQ-DOX NPs treatment did not induce any decrease in the
5 nucleic acids content. However, by increasing the concentration of SQ-DOX NPs to 5 μM ,
6 difference spectrum (c-a, Figure 6B) was marked by very high Raman intensity of bands
7 corresponding to DOX features. In addition, the intensity of 1210/1241 cm^{-1} ratio in
8 difference spectrum (c-a) decreased as compared to (b-a) (Figure 6B). Such decrease suggests
9 that released DOX is intercalated in DNA after hydrolysis.

10 We then investigated the distribution and the interaction of DOX and SQ-DOX NPs in the
11 cytoplasm of M109 treated cells. Figure 7A and 7B, showed mean Raman spectra of the
12 cytoplasm from untreated and treated cells after 1 h exposure time to either DOX or SQ-DOX
13 NPs. Raman spectra measured in the cytoplasm of cells treated with 1 μM DOX were similar
14 to those of control cells (Figure 7A). Difference spectra (Figure 7A, b-a and c-a) suggested
15 that there were no evident DOX features in the cytoplasm, meaning that DOX was
16 predominantly accumulated in the nucleus. In addition, DOX treatment did not induce
17 significant changes in the proteins and lipids cytoplasmic contents. Difference spectra were
18 then calculated for SQ-DOX NPs treatment and analyzed (Figure 7B, b-a, c-a). At 1 μM SQ-
19 DOX NPs, the profile of the difference spectrum (b-a) was similar to that observed in the case
20 of DOX treatment. When the cells were treated with 5 μM SQ-DOX, the drug was detected in
21 the cytoplasm (Figure 8B, b-a).

22 DISCUSSION

23 One of the most innovative and recent strategies in nanomedicine was the recent introduction
24 of the "squalenoylation" technology. Such strategy has allowed the emergence of new
25 treatments in cancer (42), neurological disorders (43), pain (44) and inflammation (45). The

1 “squalenoylation” method, initially developed with highly hydrophilic nucleosidic analogues
2 such as the gemcitabine (46–53) has been further extended to more hydrophobic drugs such as
3 paclitaxel(54) or doxorubicin (DOX) (18). In the case of DOX, conjugates were obtained by
4 the covalent linkage of SQ to DOX on the hydroxyl group of 14-C carbon atom (SQ-DOX)
5 allowing the formation of elongated SQ-DOX NPs in water, with a diameter of ~ 130 nm and
6 high drug loading (~ 57%) (18,55).
7
8
9
10
11
12
13

14 As shown in figure 2 and table 1, DOX was more cytotoxic than SQ-DOX NPs in M109 cells
15 *in vitro*. In fact, the IC₅₀ values of DOX were 7- and 10-times lower than the values
16 corresponding to SQ-DOX under long- and short-term treatment respectively. These data are
17 in agreement with those published earlier on MiaPaCa2 pancreatic carcinoma cells, which
18 suggested that this differential effect was due to the fact that the drug needs to be released to
19 be active (18). To investigate whether such cytotoxic effect was associated to an apoptotic
20 effect, annexin V staining and caspase-3/7 activity were evaluated. Both DOX and SQ-DOX
21 NPs were able to induce apoptosis (Figure 2c and d). As expected, DOX displayed a higher
22 level of apoptosis markers than SQ-DOX NPs. Altogether, cytotoxic and apoptotic data
23 suggest that *in vitro*, DOX is more active than SQ-DOX NPs. However, it is important to note
24 that the main advantage of SQ-DOX NPs lies in their efficacy *in vivo* where a reduction of
25 blood clearance and urinary excretion was observed together with higher tumor concentration
26 of the drug (18).
27
28
29
30
31
32
33
34
35
36
37
38
39
40
41
42
43
44
45
46

47 As the aim was to investigate the incorporation and the cellular distribution of DOX and SQ-
48 DOX NPs, we first analyzed such parameters using confocal fluorescence microscopy and
49 microspectrofluorometry. As shown in figure 3, DOX accumulated predominantly in the cell
50 nucleus. The fact that the fluorescence emission remained modest resulted from the quenching
51 of the fluorescence emission upon intercalation of DOX in DNA (40). Similarly, a red
52 fluorescence emission was also observed in the cell nuclei after treatment with SQ-DOX NPs.
53
54
55
56
57
58
59
60
61
62
63
64
65

1 At the opposite of DOX, drug conjugate emission was also observed in the cytoplasm,
2 suggesting that the hydrolysis of SQ-DOX NPs was necessary before the diffusion of DOX
3 into the nucleus. At this stage, confocal fluorescence microscopy analysis did not allow to
4 distinguish between DOX and SQ-DOX NPs in the different cellular compartments. On the
5 other hand, previous quantitative studies, carried out using microspectrofluorometry, have
6 provided evidence that the nuclear uptake of DOX correlated with its cytotoxic effect (39). In
7 fact, such technique allows the quantification of DOX concentration bound to DNA into the
8 nucleus (40). We thus carried out the quantification of the drug incorporation by
9 measurements of fluorescence emission spectra of both drug forms and evaluated their
10 intensities. The fluorescence emission intensity in the cell nuclei was higher after SQ-DOX
11 NPs treatment when compared to DOX (figure 4), whereas the cytotoxic and apoptotic effects
12 of DOX were at the opposite higher (figures 2). In order to characterize and quantify these
13 two forms of the drug at the molecular level, we subsequently analyzed their incorporation
14 and cellular distribution by Raman microspectroscopy.

15 Raman microspectroscopy allowed the analysis of the cellular drug distribution and the
16 cellular biochemical changes upon treatment with DOX and SQ-DOX NPs. At a
17 concentration of 5 μM , the intensity of Raman bands of DOX in the nucleus at 1210, 1241
18 cm^{-1} clearly appeared in the difference spectrum between treated and untreated cells,
19 indicating nuclear incorporation of the drug (Figure 6). Moreover, the intensity of 1210/1241
20 cm^{-1} ratio decreased compared to DOX in solution, suggesting the intercalation of DOX in
21 DNA. We have previously reported that this intercalation of DOX between base pairs of DNA
22 was characterized by other changes related to the decrease in the intensities of the bands at
23 1226 cm^{-1} , and 1255 cm^{-1} , and at 1461 cm^{-1} (27). In addition, DOX treated cells exhibited a
24 decrease in nucleic acid content which is consistent with its mechanism of action, related to
25 DNA synthesis inhibition (56, 57). Such mechanisms include the inhibition of topoisomerase

1
2
3
4
5
6
7
8
9
10
11
12
13
14
15
16
17
18
19
20
21
22
23
24
25
26
27
28
29
30
31
32
33
34
35
36
37
38
39
40
41
42
43
44
45
46
47
48
49
50
51
52
53
54
55
56
57
58
59
60
61
62
63
64
65

II activity upon its binding to DNA in a ternary complex (57). This latter is consequently able to inhibit DNA replication. In addition, the effect of DOX treatment was associated with an increase in the proteins content, which was in agreement with data reported earlier (58).

After 1 μM treatment, data showed that Raman bands intensities attributed mainly to DOX were higher in the cell nuclei after SQ-DOX NPs treatment when compared to DOX. Moreover, these bands were observed only in the cytoplasm of cells treated with SQ-DOX NPs. When cells were treated with 5 μM SQ-DOX, the intensities of these Raman bands increased markedly both in the cytoplasm and the nucleus. In addition, the intensity of the 1210/1244 cm^{-1} ratio decreased when compared to the treatment at a concentration of 1 μM , suggesting that a fraction of hydrolyzed SQ-DOX was intercalated between base pairs of DNA. Unlike DOX, SQ-DOX NPs treatment did not induce detectable decrease in the nucleic acids contents, which is in agreement with the lowest cytotoxicity and apoptosis data.

Maksimenko *et al.* described that the internalization of SQ-DOX into the cells occurred via endocytosis. The intracellular release of DOX from SQ-DOX NPs results from the hydrolysis of the prodrug in lysosomes by esterases as reported earlier (18). The released drug is then incorporated into the nucleus, allowing the induction of its biological effects. Our data clearly show the presence of SQ in the cytoplasm, as it was expected. In fact, the band at 1669 cm^{-1} , which is specific to SQ, was observed in the difference spectrum recorded from the cytoplasm of cells treated with SQ-DOX NPs and non-treated ones (Figure 7B). Interestingly, this band was also detected in the nucleus of M109 cells treated with SQ-DOX NPs, suggesting that the bioconjugate was probably able to diffuse into the nucleus (Figure 6B). We then asked whether this observation could help to understand the discrepancy between the drug fluorescence emission data observed in the nucleus and its biological effects. We thus analyzed the interaction of SQ-DOX molecules with DNA in solution using surface enhanced Raman scattering (SERS) to verify if SQ-DOX was able (or not) to intercalate into the DNA.

1 SERS spectra of SQ-DOX alone and in the presence of DNA with various ratios were
2 measured. As shown in supplementary figure S1 and at the opposite of DOX, the comparison
3
4 between spectra of SQ-DOX, free and complexed to DNA at different molar ratio, did not
5
6 show any changes in the markers of DNA intercalation.. In other words, DNA intercalation
7
8 should only occur in the case of released DOX after SQ-DOX hydrolysis. This finding could
9
10 explain the the lower cytotoxicity and apoptosis effects in the case of SQ-DOX NPs treatment.
11
12 In fact, the Raman signal of the drug in the nucleus (Figure 6) could be a combination of
13
14 DOX and SQ-DOX spectral features but only the fraction of DOX released from SQ-DOX
15
16 could intercalate into the DNA (Figure 6B), as confirmed in part by the relative decrease in
17
18 the intensity 1210/1244 cm^{-1} ratio (Figure 6B). After 5 h treatment with SQ-DOX at 5 μM ,
19
20 the Raman spectral features showed a higher 1210/1244 cm^{-1} ratio in the nucleus, suggesting a
21
22 lowest fraction of the intercalated form of DOX and a higher fraction of the non-hydrolyzed
23
24 form of SQ-DOX (Figure 8a).
25
26
27
28
29
30

31 CONCLUSION

32
33 This study demonstrated the potential of Raman spectroscopy as a label free technique for the
34
35 *in vitro* characterization of the chemotherapeutic agents and their prodrug forms in single
36
37 living cancer cell. Our data provided simultaneous information on the detection of the
38
39 different forms of DOX and SQ-DOX NPs, and the identification of biochemical changes.
40
41 Distinct Raman spectroscopic markers of these chemotherapeutic agents were identified and
42
43 used to help to understand the mechanisms involved in the efficacy of the drugs *in vitro*. In
44
45 conclusion, this study brings additional information to the knowledge of nanomedicine field.
46
47
48
49
50

51 ACKNOWLEDGEMENTS

52
53 The authors would like to thank the Platform of Cellular and Tissular Imaging (PICT) for
54
55 the equipment availability.
56
57
58
59
60
61
62
63
64
65

AUTHOR CONTRIBUTIONS

1
2 PC, HM and AB: Conception and design; FD, BS, and AM: synthesis and characterization of
3
4 nanoparticles SQ-DOX; HR, LVG, AA, and AB: Methodology and data acquisition ; HR,
5
6 HM and AB: Data analysis and manuscript writing; SM, DD, and PC: Discussion and
7
8 revision.
9

10
11
12 **Disclosure Statement:** PC is the founder of Squal Pharma, a start-up dedicated to the
13
14 development of squalenoylated nanomedicines. All other authors have nothing to disclose.
15
16

17
18
19
20
21 **Availability of data and materials:** All data generated or analyzed during this study are
22
23 included in this published article [and its supplementary information files]. If not, they are
24
25 available from the corresponding author on reasonable request.
26

27
28
29 **Funding:** This research did not receive any specific grant from funding agencies in the public,
30
31 commercial, or not-for-profit sectors.
32

REFERENCES

- 33
34
35
36
37 1. Higgins GS, O’Cathail SM, Muschel RJ, McKenna WG. Drug radiotherapy
38 combinations: review of previous failures and reasons for future optimism. *Cancer Treat*
39 *Rev.* 2015 Feb;41(2):105–13.
40
41 2. Tacar O, Sriamornsak P, Dass CR. Doxorubicin: an update on anticancer molecular
42 action, toxicity and novel drug delivery systems. *J Pharm Pharmacol.* 2013
43 Feb;65(2):157–70.
44
45 3. Arcamone F. Properties of antitumor anthracyclines and new developments in their
46 application: Cain memorial award lecture. *Cancer Res.* 1985 Dec;45(12 Pt 1):5995–9.
47
48 4. Meredith A-M, Dass CR. Increasing role of the cancer chemotherapeutic doxorubicin in
49 cellular metabolism. *J Pharm Pharmacol.* 2016 Jun;68(6):729–41.
50
51 5. Thorn CF, Oshiro C, Marsh S, Hernandez-Boussard T, McLeod H, Klein TE, et al.
52 Doxorubicin pathways: pharmacodynamics and adverse effects. *Pharmacogenetics and*
53 *Genomics.* 2011 Jul;21(7):440–6.
54
55 6. Yang F, Teves SS, Kemp CJ, Henikoff S. Doxorubicin, DNA torsion, and chromatin
56 dynamics. *Biochimica et Biophysica Acta (BBA) - Reviews on Cancer.* 2014
57 Jan;1845(1):84–9.
58
59
60
61
62
63
64
65

- 1
2
3
4
5
6
7
8
9
10
11
12
13
14
15
16
17
18
19
20
21
22
23
24
25
26
27
28
29
30
31
32
33
34
35
36
37
38
39
40
41
42
43
44
45
46
47
48
49
50
51
52
53
54
55
56
57
58
59
60
61
62
63
64
65
7. Deavall DG, Martin EA, Horner JM, Roberts R. Drug-Induced Oxidative Stress and Toxicity. *Journal of Toxicology*. 2012;2012:1–13.
8. Wang S, Konorev EA, Kotamraju S, Joseph J, Kalivendi S, Kalyanaraman B. Doxorubicin Induces Apoptosis in Normal and Tumor Cells via Distinctly Different Mechanisms: INTERMEDIACY OF H₂O₂- AND p53-DEPENDENT PATHWAYS. *Journal of Biological Chemistry*. 2004 Jun 11;279(24):25535–43.
9. Pommier Y, Leo E, Zhang H, Marchand C. DNA Topoisomerases and Their Poisoning by Anticancer and Antibacterial Drugs. *Chemistry & Biology*. 2010 May;17(5):421–33.
10. Tan HH, Porter AG. DNA methyltransferase I is a mediator of doxorubicin-induced genotoxicity in human cancer cells. *Biochemical and Biophysical Research Communications*. 2009 May;382(2):462–7.
11. Yokochi T. Doxorubicin Inhibits DNMT1, Resulting in Conditional Apoptosis. *Molecular Pharmacology*. 2004 Aug 31;66(6):1415–20.
12. Carvalho C, Santos R, Cardoso S, Correia S, Oliveira P, Santos M, et al. Doxorubicin: The Good, the Bad and the Ugly Effect. *Current Medicinal Chemistry*. 2009 Sep 1;16(25):3267–85.
13. Octavia Y, Tocchetti CG, Gabrielson KL, Janssens S, Crijns HJ, Moens AL. Doxorubicin-induced cardiomyopathy: From molecular mechanisms to therapeutic strategies. *Journal of Molecular and Cellular Cardiology*. 2012 Jun;52(6):1213–25.
14. Brigger I, Dubernet C, Couvreur P. Nanoparticles in cancer therapy and diagnosis. *Advanced Drug Delivery Reviews*. 2002 Sep;54(5):631–51.
15. Cho K, Wang X, Nie S, Chen Z, Shin DM. Therapeutic Nanoparticles for Drug Delivery in Cancer. *Clinical Cancer Research*. 2008 Mar 1;14(5):1310–6.
16. Horcajada P, Chalati T, Serre C, Gillet B, Sebrie C, Baati T, et al. Porous metal–organic-framework nanoscale carriers as a potential platform for drug delivery and imaging. *Nature Materials*. 2010 Feb;9(2):172–8.
17. Shi J, Kantoff PW, Wooster R, Farokhzad OC. Cancer nanomedicine: progress, challenges and opportunities. *Nature Reviews Cancer*. 2016 Nov 11;17(1):20–37.
18. Maksimenko A, Dosio F, Mougín J, Ferrero A, Wack S, Reddy LH, et al. A unique squalenoylated and nonpegylated doxorubicin nanomedicine with systemic long-circulating properties and anticancer activity. *Proc Natl Acad Sci USA*. 2014 Jan 14;111(2):E217–226.
19. Bae YH, Park K. Targeted drug delivery to tumors: myths, reality and possibility. *J Control Release*. 2011 Aug 10;153(3):198–205.
20. Mallidis C, Sanchez V, Wistuba J, Wuebbeling F, Burger M, Fallnich C, et al. Raman microspectroscopy: shining a new light on reproductive medicine. *Hum Reprod Update*. 2014 Jun;20(3):403–14.

- 1 21. Neugebauer U, Rösch P, Popp J. Raman spectroscopy towards clinical application: drug
2 monitoring and pathogen identification. *International Journal of Antimicrobial Agents*.
3 2015 Dec;46:S35–9.
- 4 22. Gala de Pablo J, Armistead FJ, Peyman SA, Bonthron D, Lones M, Smith S, et al.
5 Biochemical fingerprint of colorectal cancer cell lines using label-free live single-cell
6 Raman spectroscopy. *Journal of Raman Spectroscopy*. 2018 Aug;49(8):1323–32.
- 7 23. Guo J, Cai W, Du B, Qian M, Sun Z. Raman spectroscopic investigation on the
8 interaction of malignantheptocytes with doxorubicin. *Biophysical Chemistry*. 2009
9 Mar;140(1–3):57–61.
- 10 24. Schie IW, Alber L, Gryshuk AL, Chan JW. Investigating drug induced changes in
11 single, living lymphocytes based on Raman micro-spectroscopy. *The Analyst*.
12 2014;139(11):2726–33.
- 13 25. Short KW, Carpenter S, Freyer JP, Mourant JR. Raman Spectroscopy Detects
14 Biochemical Changes Due to Proliferation in Mammalian Cell Cultures. *Biophys J*. 2005
15 Jun;88(6):4274–88.
- 16 26. Swain RJ, Stevens MM. Raman microspectroscopy for non-invasive biochemical
17 analysis of single cells. *Biochem Soc Trans*. 2007 Jun;35(Pt 3):544–9.
- 18 27. Beljebbar A, Sockalingum GD, Angiboust JF, Manfait M. Comparative FT SERS,
19 resonance Raman and SERRS studies of doxorubicin and its complex with DNA.
20 *Spectrochimica Acta Part A: Molecular and Biomolecular Spectroscopy*. 1995
21 Nov;51(12):2083–90.
- 22 28. Byrne HJ, Bonnier F, Casey A, Maher M, McIntyre J, Efeoglu E, et al. Advancing
23 Raman microspectroscopy for cellular and subcellular analysis: towards in vitro high-
24 content spectralomic analysis. *Appl Opt*. 2018 Aug 1;57(22):E11–9.
- 25 29. Das G, Nicastrì A, Coluccio ML, Gentile F, Candeloro P, Cojoc G, et al. FT-IR, Raman,
26 RRS measurements and DFT calculation for doxorubicin. *Microscopy Research and
27 Technique*. 2010;NA-NA.
- 28 30. Farhane Z, Bonnier F, Byrne HJ. An in vitro study of the interaction of the
29 chemotherapeutic drug Actinomycin D with lung cancer cell lines using Raman micro-
30 spectroscopy. *J Biophotonics*. 2018 Jan;11(1).
- 31 31. Farhane Z, Bonnier F, Howe O, Casey A, Byrne HJ. Doxorubicin kinetics and effects on
32 lung cancer cell lines using in vitro Raman micro-spectroscopy: binding signatures, drug
33 resistance and DNA repair. *J Biophotonics*. 2018 Jan;11(1).
- 34 32. Manfait M, Alix AJ, Jeannesson P, Jardillier JC, Theophanides T. Interaction of
35 adriamycin with DNA as studied by resonance Raman spectroscopy. *Nucleic Acids Res*.
36 1982 Jun 25;10(12):3803–16.
- 37 33. Moritz TJ, Taylor DS, Krol DM, Fritch J, Chan JW. Detection of doxorubicin-induced
38 apoptosis of leukemic T-lymphocytes by laser tweezers Raman spectroscopy.
39 *Biomedical Optics Express*. 2010 Nov 1;1(4):1138.

34. Lê LMM, Berge M, Tfayli A, Zhou J, Prognon P, Baillet-Guffroy A, et al. Rapid discrimination and quantification analysis of five antineoplastic drugs in aqueous solutions using Raman spectroscopy. *European Journal of Pharmaceutical Sciences*. 2018 Jan;111:158–66.
35. Birech Z, Mwangi PW, Bukachi F, Mandela KM. Application of Raman spectroscopy in type 2 diabetes screening in blood using leucine and isoleucine amino-acids as biomarkers and in comparative anti-diabetic drugs efficacy studies. *PLoS ONE*. 2017;12(9):e0185130.
36. Bourget P, Amin A, Vidal F, Merlette C, Troude P, Baillet-Guffroy A. The contribution of Raman spectroscopy to the analytical quality control of cytotoxic drugs in a hospital environment: eliminating the exposure risks for staff members and their work environment. *Int J Pharm*. 2014 Aug 15;470(1–2):70–6.
37. Nawaz H, Bonnier F, Knief P, Howe O, Lyng FM, Meade AD, et al. Evaluation of the potential of Raman microspectroscopy for prediction of chemotherapeutic response to cisplatin in lung adenocarcinoma. *The Analyst*. 2010;135(12):3070.
38. Gigli M, Rasoanaivo TW, Millot JM, Jeannesson P, Rizzo V, Jardillier JC, et al. Correlation between growth inhibition and intranuclear doxorubicin and 4'-deoxy-4'-iododoxorubicin quantitated in living K562 cells by microspectrofluorometry. *Cancer Res*. 1989 Feb 1;49(3):560–4.
39. Morjani H, Millot JM, Belhoussine R, Sebille S, Manfait M. Anthracycline subcellular distribution in human leukemic cells by microspectrofluorometry: factors contributing to drug-induced cell death and reversal of multidrug resistance. *Leukemia*. 1997 Jul;11(7):1170–9.
40. Gigli M, Doglia SM, Millot JM, Valentini L, Manfait M. Quantitative study of doxorubicin in living cell nuclei by microspectrofluorometry. *Biochimica et Biophysica Acta (BBA) - Gene Structure and Expression*. 1988 May;950(1):13–20.
41. Chun HJ, Weiss TL, Devarenne TP, Laane J. Vibrational spectra and DFT calculations of squalene. *Journal of Molecular Structure*. 2013 Jan;1032:203–6.
42. Kotelevets L, Chastre E, Caron J, Mouglin J, Bastian G, Pineau A, et al. A Squalene-Based Nanomedicine for Oral Treatment of Colon Cancer. *Cancer Research*. 2017 Jun 1;77(11):2964–75.
43. Gaudin A, Yemisci M, Eroglu H, Lepetre-Mouelhi S, Turkoglu OF, Dönmez-Demir B, et al. Squalenoyl adenosine nanoparticles provide neuroprotection after stroke and spinal cord injury. *Nature Nanotechnology*. 2014 Dec;9(12):1054–62.
44. Feng J, Lepetre-Mouelhi S, Gautier A, Mura S, Cailleau C, Coudore F, et al. A new painkiller nanomedicine to bypass the blood-brain barrier and the use of morphine. *Science Advances*. 2019 Feb;5(2):eaau5148.
45. Dormont F, Brusini R, Cailleau C, Reynaud F, Peramo A, Gendron A, et al. Squalene-based multidrug nanoparticles for improved mitigation of uncontrolled inflammation in rodents. *Science Advances*. 2020 Jun;6(23):eaaz5466.

- 1
2
3
4
5
6
7
8
9
10
11
12
13
14
15
16
17
18
19
20
21
22
23
24
25
26
27
28
29
30
31
32
33
34
35
36
37
38
39
40
41
42
43
44
45
46
47
48
49
50
51
52
53
54
55
56
57
58
59
60
61
62
63
64
65
46. Couvreur P, Stella B, Reddy LH, Hillaireau H, Dubernet C, Desmaële D, et al. Squalenoyl Nanomedicines as Potential Therapeutics. *Nano Letters*. 2006 Nov;6(11):2544–8.
 47. Desmaële D, Gref R, Couvreur P. Squalenoylation: A generic platform for nanoparticulate drug delivery. *Journal of Controlled Release*. 2012 Jul;161(2):609–18.
 48. Reddy LH, Renoir J-M, Marsaud V, Lepetre-Mouelhi S, Desmaële D, Couvreur P. Anticancer Efficacy of Squalenoyl Gemcitabine Nanomedicine on 60 Human Tumor Cell Panel and on Experimental Tumor. *Molecular Pharmaceutics*. 2009 Oct 5;6(5):1526–35.
 49. Reddy LH, Khoury H, Paci A, Deroussent A, Ferreira H, Dubernet C, et al. Squalenoylation Favorably Modifies the in Vivo Pharmacokinetics and Biodistribution of Gemcitabine in Mice. *Drug Metabolism and Disposition*. 2008 Aug;36(8):1570–7.
 50. Reddy LH, Marque P-E, Dubernet C, Mouelhi S-L, Desmaële D, Couvreur P. Preclinical Toxicology (Subacute and Acute) and Efficacy of a New Squalenoyl Gemcitabine Anticancer Nanomedicine. *Journal of Pharmacology and Experimental Therapeutics*. 2008 May;325(2):484–90.
 51. Reddy LH, Dubernet C, Mouelhi SL, Marque PE, Desmaele D, Couvreur P. A new nanomedicine of gemcitabine displays enhanced anticancer activity in sensitive and resistant leukemia types. *Journal of Controlled Release*. 2007 Dec;124(1–2):20–7.
 52. Sobot D, Mura S, Rouquette M, Vukosavljevic B, Cayre F, Buchy E, et al. Circulating Lipoproteins: A Trojan Horse Guiding Squalenoylated Drugs to LDL-Accumulating Cancer Cells. *Mol Ther*. 2017 05;25(7):1596–605.
 53. Sobot D, Mura S, Yesylevskyy SO, Dalbin L, Cayre F, Bort G, et al. Conjugation of squalene to gemcitabine as unique approach exploiting endogenous lipoproteins for drug delivery. *Nat Commun*. 2017 30;8:15678.
 54. Caron J, Maksimenko A, Wack S, Lepeltier E, Bourgaux C, Morvan E, et al. Improving the Antitumor Activity of Squalenoyl-Paclitaxel Conjugate Nanoassemblies by Manipulating the Linker between Paclitaxel and Squalene. *Advanced Healthcare Materials*. 2013 Jan;2(1):172–85.
 55. Mougín J, Yesylevskyy SO, Bourgaux C, Chapron D, Michel J-P, Dosio F, et al. Stacking as a Key Property for Creating Nanoparticles with Tunable Shape: The Case of Squalenoyl-Doxorubicin. *ACS Nano*. 2019 Nov 26;13(11):12870–9.
 56. Nawaz H, Garcia A, Meade AD, Lyng FM, Byrne HJ. Raman micro spectroscopy study of the interaction of vincristine with A549 cells supported by expression analysis of bcl-2 protein. *Analyst*. 2013;138(20):6177.
 57. Komiyama T, Oki T, Inui T. Interaction of new anthracycline antibiotics with DNA. Effects on nucleic acid synthesis and binding to DNA. *Biochimica et Biophysica Acta (BBA) - Gene Structure and Expression*. 1983 May 20;740(1):80–7.

- 1 58. Farhane Z, Bonnier F, Byrne HJ. Monitoring doxorubicin cellular uptake and trafficking
2 using in vitro Raman microspectroscopy: short and long time exposure effects on lung
3 cancer cell lines. *Analytical and Bioanalytical Chemistry*. 2017 Feb;409(5):1333–46.
- 4 59. Wolthuis R, Bakker Schut TC, Caspers PJ, Buschman HPJ, Romer TJ, Bruining HA, et
5 al. In *Fluorescent and Luminescent Probes for Biological Activity*. Mason, WT, Ed.
6 1999;433–455.
- 7 60. Barnes RJ, Dhanoa MS, Lister SJ. Standard Normal Variate Transformation and De-
8 trending of Near-Infrared Diffuse Reflectance Spectra. *Appl Spectrosc, AS*. 1989 May
9 1;43(5):772–7.

10
11
12
13
14
15
16
17
18
19
20
21
22
23
24
25
26
27
28
29
30
31
32
33
34
35
36
37
38
39
40
41
42
43
44
45
46
47
48
49
50
51
52
53
54
55
56
57
58
59
60
61
62
63
64
65

Legend figure

Figure 1: Subcellular localization of DOX and SQ-DOX in single living M109 cell by Raman microspectroscopy

Figure 2: Antitumor activity of DOX and SQ-DOX on M109 cell growth (a and b) and apoptosis (c and d). For cell growth inhibition, cells were treated with concentrations ranging from 0.1 nM to 1 μ M for a) 72h time exposure and b) 1h treatment and 72h post-incubation after washing. For apoptosis, flow cytometry analysis of (c) Annexin V and (d) Caspase 3/7 expressed by the percentage of M109 apoptotic positive cells assessed using the Muse Annexin V and Caspase 3/7 assay kit. Cell growth rate is expressed as percentage compared to untreated cells control; error bars indicating standard deviation of three duplicated independent measurements. For apoptosis, values represent the mean \pm SEM of three independent experiments (n=3, Mann & Whitney test).

Figure 3: Bright field imaged of M109 cells (a and b) and fluorescence microscopy images of cells treated with DOX and SQ-DOX at concentration of 1 μ M for 1h exposure timesubcellular distribution. Fluorescence microscopy images of M109 cells showing the cellular uptake of DOX or SQ-DOX after 1h of treatment (1 μ M). Nuclei were stained in blue with Hoechst33342 (c and d), Doxorubicin in red (e and f), and overlay of the three images (g and h). (x40, scale bar = 20 μ m).

Figure 4: DOX nuclear uptake after DOX and SQ-DOX treatments. Time course of doxorubicin cell uptake and internalization after 1h of SQ-DOX or DOX treatment, as measured by confocal laser microspectrofluorometry (n=3, mean \pm SD).

Figure 5: Chemical structure of a) DOX, b) SQ, c) SQ-DOX, and d) their Raman spectra in solutions.

Figure 6: Mean Raman spectra measured on untreated cell nucleus (a) and nucleus treated for 1 h with DOX (panel A) and SQ-DOX (panel B) with concentrations of: b) 1 μ M, and c) 5 μ M. 10 spectra were measured on each cell nucleus with an acquisition time of 10 seconds in the fingerprint region 570-1800 cm^{-1} . The shaded areas represent the respective standard deviations. Difference spectra (b-a, c-a) were obtained by subtracting Raman spectra treated cell with concentration of 1 μ M and 5 μ M from untreated cells.

Figure 7: Mean Raman spectra measured on untreated cell cytoplasm (a) and cytoplasm treated for 1 h with DOX (panel A) and SQ-DOX (panel B) with concentrations of: b) 1 μ M, c) 5 μ M. 10 spectra were measured on each cell cytoplasm with an acquisition time of 10 seconds in the fingerprint region 570-1800 cm^{-1} . The shaded areas represent the respective standard deviations. Difference spectra (b-a, c-a) were obtained by subtracting Raman spectra treated cell with concentration of 1 μ M and 5 μ M from untreated cells.

Figure 8: Mean Raman spectra measured on nucleus (panel A) and cytoplasm (pane B) on untreated cell (a) and treated 5 h with SQ-DOX at concentration of 5 μ M (b). Difference spectra (b-a) was obtained by subtracting Raman spectra treated cell with concentration of 5 μ M from untreated cells. The shaded areas represent the respective standard deviations.

	IC ₅₀		IC ₅₀ SQ-DOX / IC ₅₀ DOX
	SQ-DOX	DOX	
72 h treatment (nM)	18.00	2.60	7
1 h treatment (μM)	1.20	0.12	10

Table 1: DOX/SQ and DOX calculated IC₅₀ values upon M109 cells long time exposure (72 h) and short time exposure (24 h + 72 h post-incubation).

DOX

Band frequency	Assignment
993	C-H ₂ , δ C=O, δ C-OH
1084	γ Ring, ω C-H ₂ , γ C-OH, ω C-H ₃
1210	δ O-H...O, ring, out C-H ₂ , δ C-OH, N-H ₂
1241	C-H ₂ , O-H, C-O-C
1302	δ O-H...O, Ring, δ C-OH, δ C-H,
1413	γ Ring, O-H, C-H ₂ , δ C-H, out N-H ₂ ,
1443	Ring, Ring-O, δ N-H, Ring=O, δ C-H, δ C-H ₂
1573	Ring, Ring(Phe)
1586	Ring
1638	C=O

Cell

Band frequency	Assignment
784	O-P-O symmetric stretching
853	Ring breathing Tyr
938	C-C bonds of peptide backbone
1004	Phenylalanine breathing mode of
1033	Phenylalanine: C-N
1096	PO ₂ ⁻ symmetric stretching
1129	C-C asymmetric stretching
1210	C-C stretch, C-H bending
1252	Amide III, C-H Bend
1305	Amide III
1341	Adenine, Phenylalanine, CH deformation
1451	CH ₃ , CH ₂ deformation
1582	Guanine, Adenine
1662	Amide I

Table 2: Tentative band assignment of the Raman signatures of DOX and untreated M109 cell

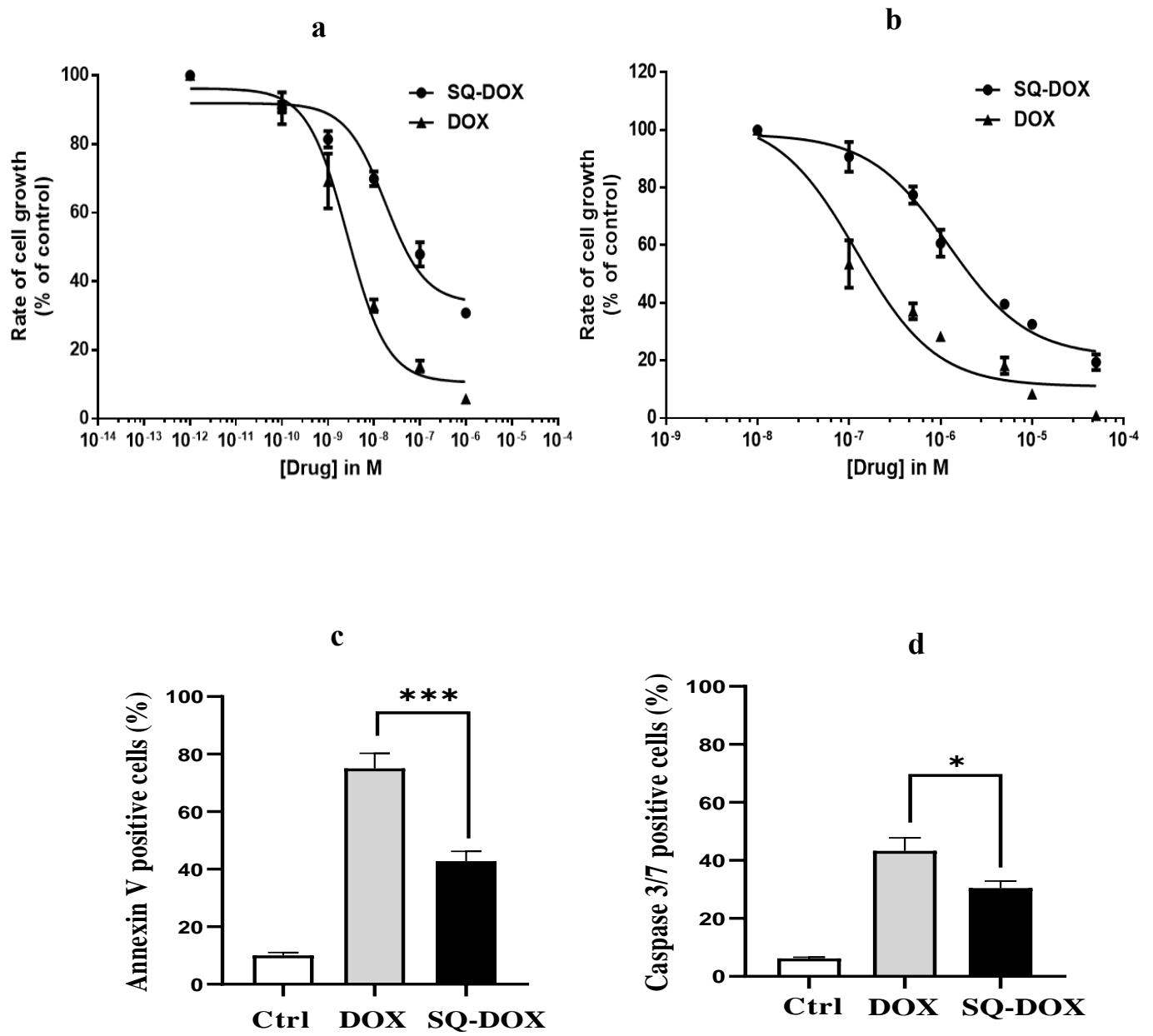


Figure 2

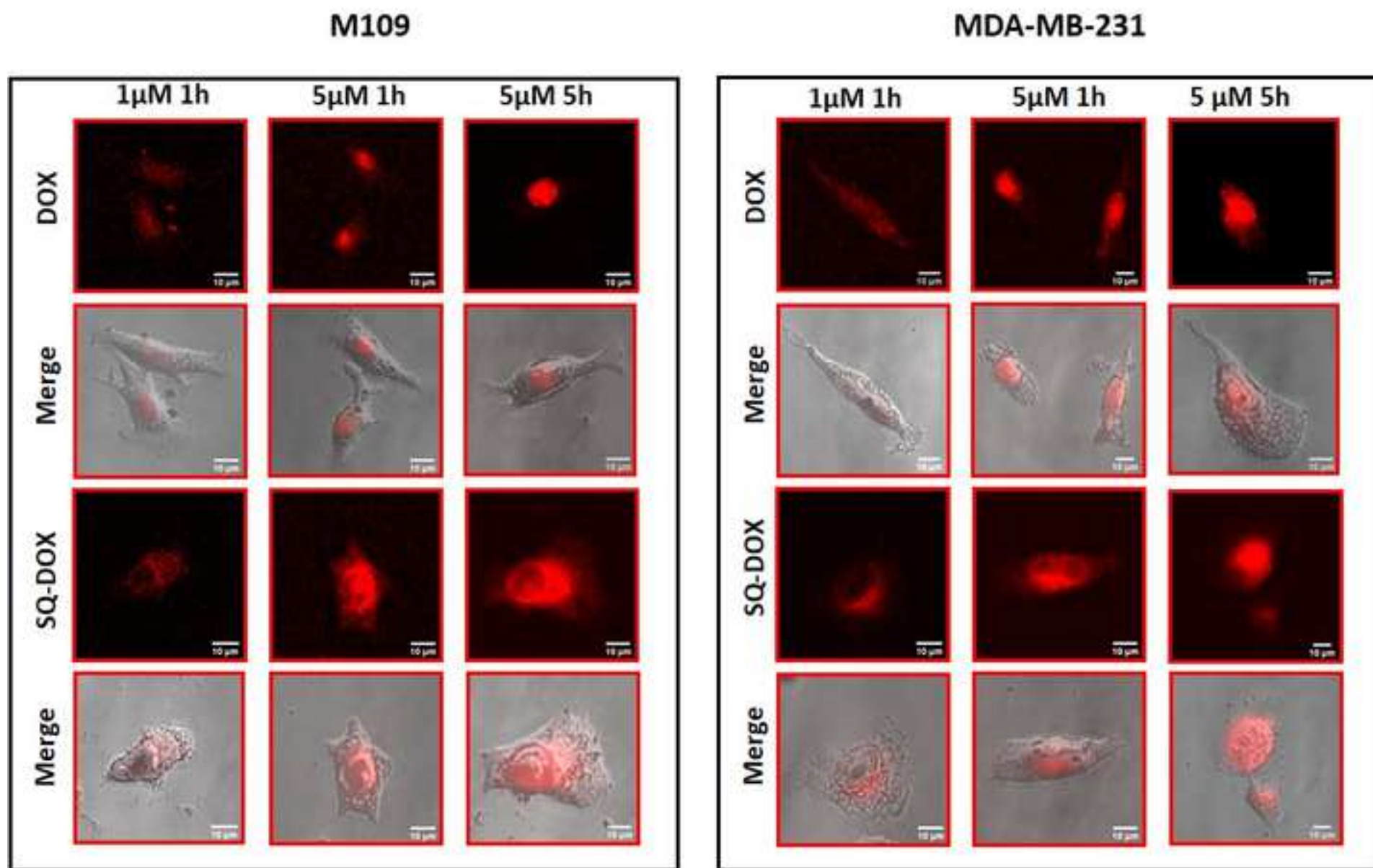


Figure 2

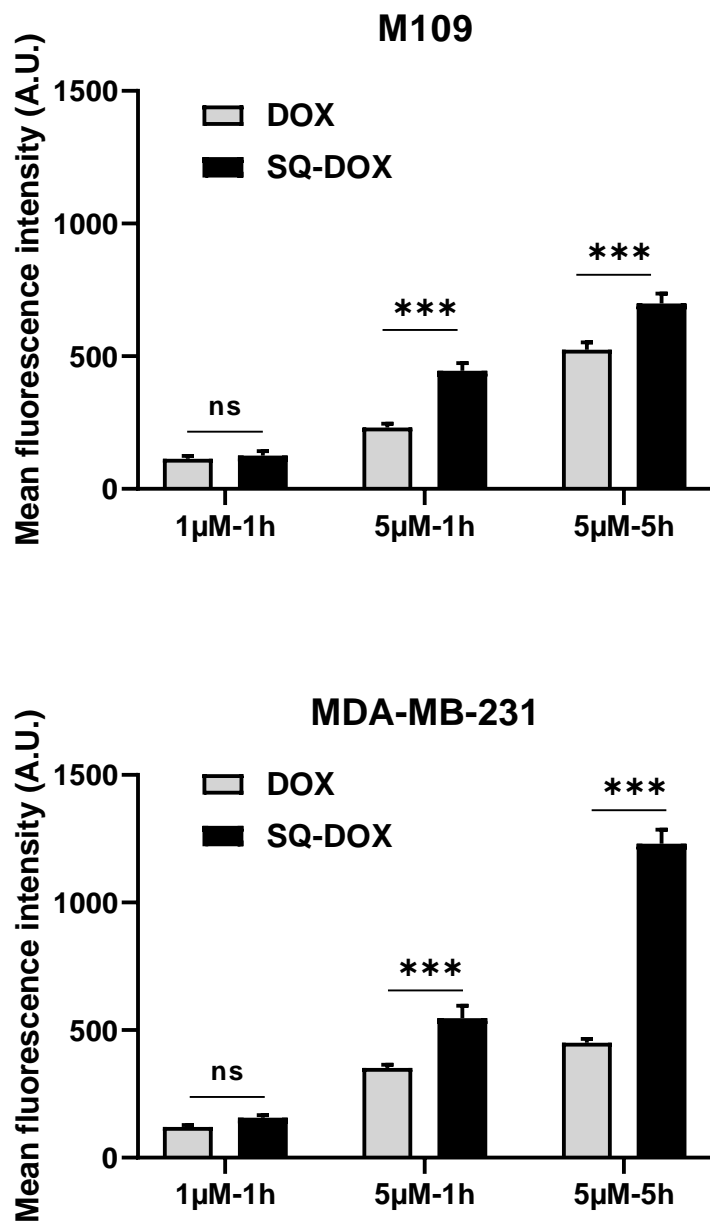


Figure 3

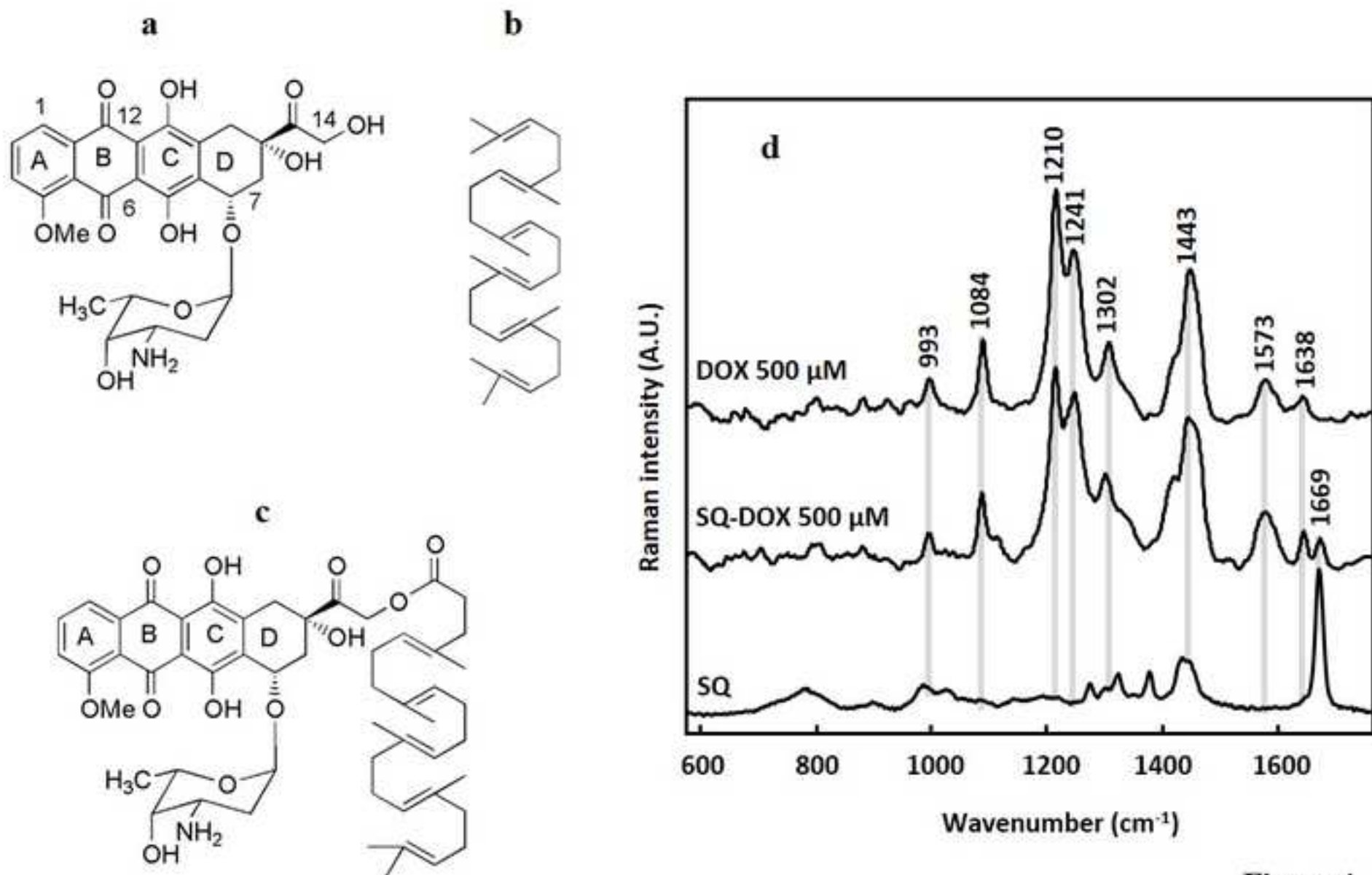


Figure 4

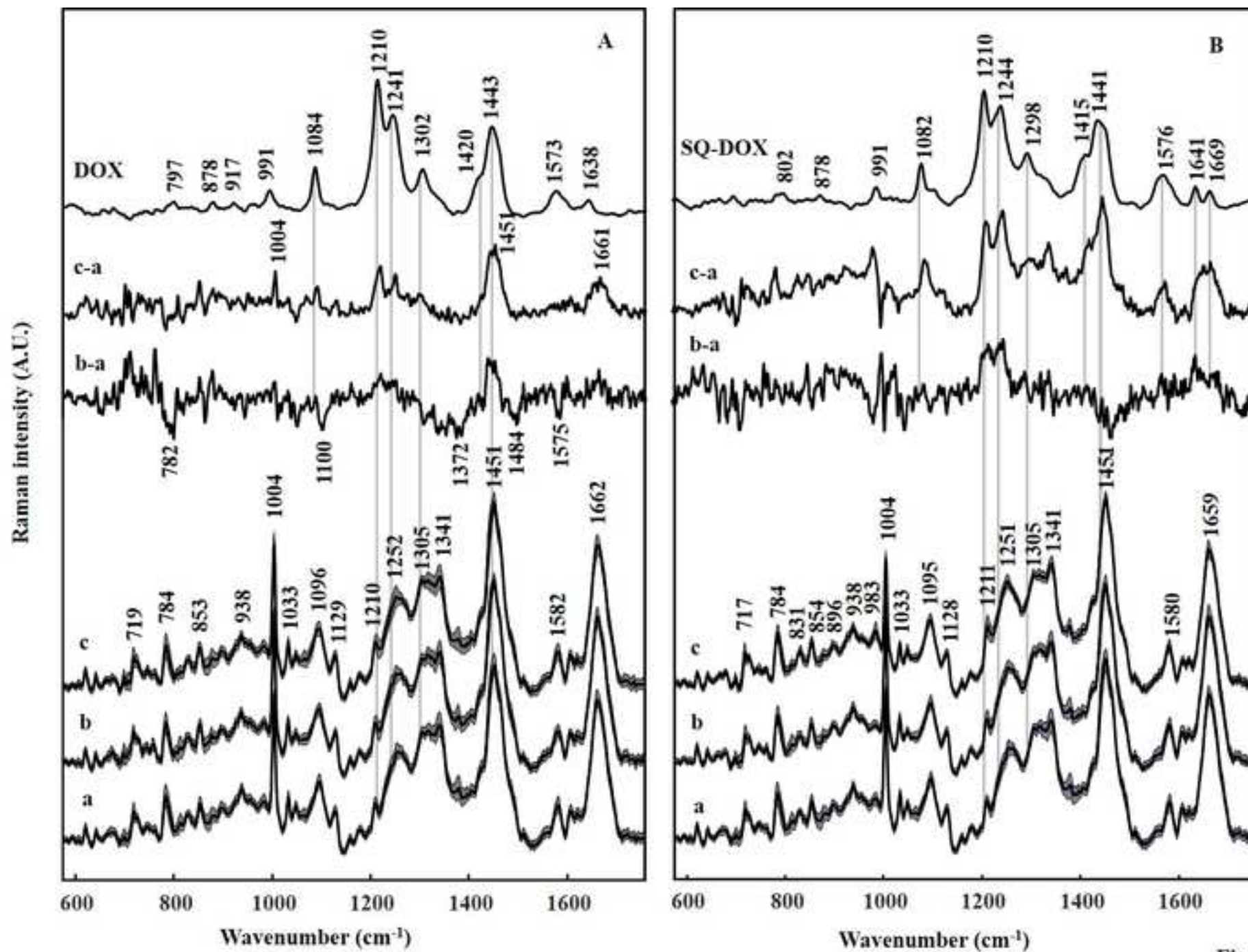


Figure 5

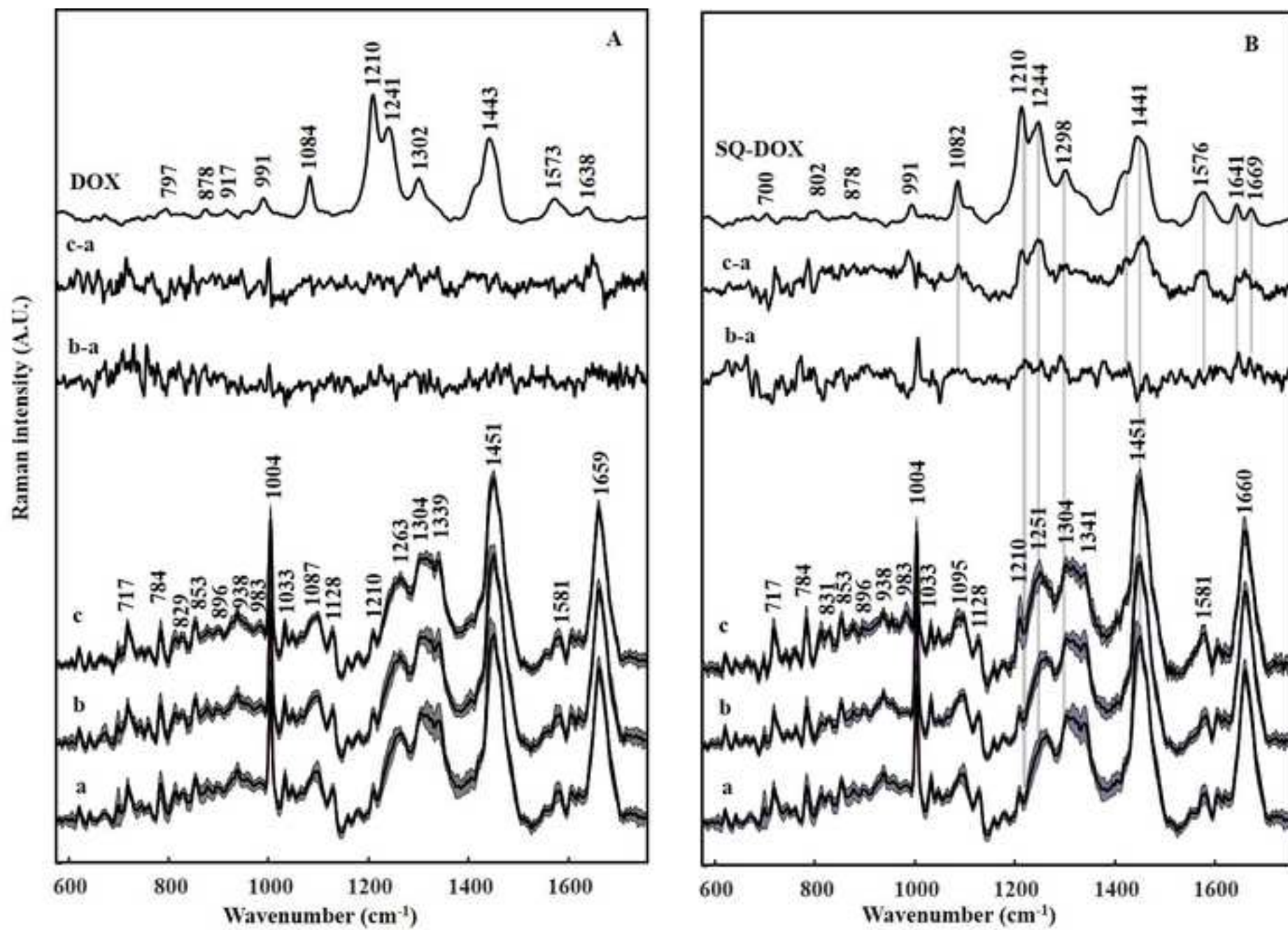


Figure 6

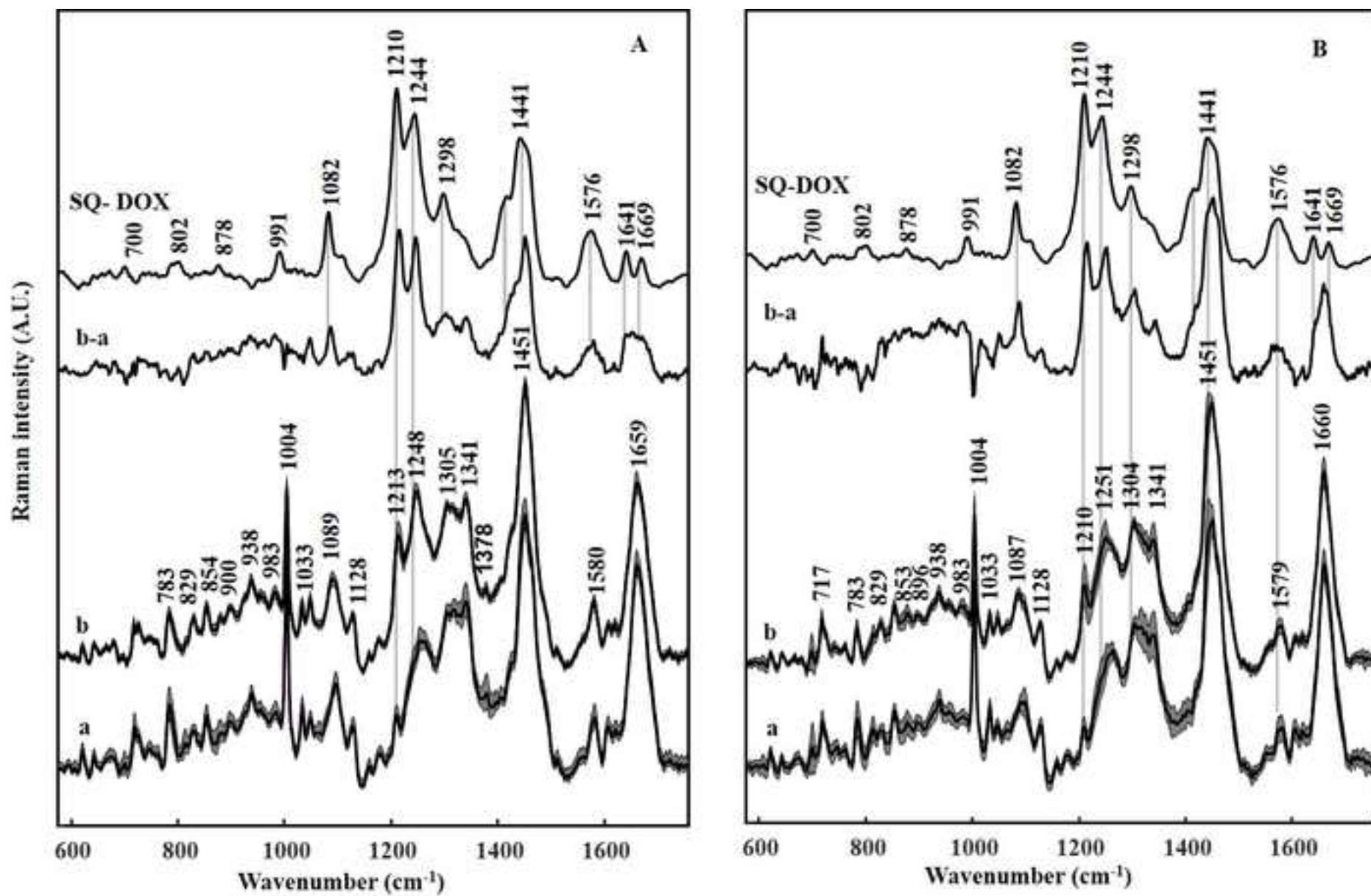


Figure 7

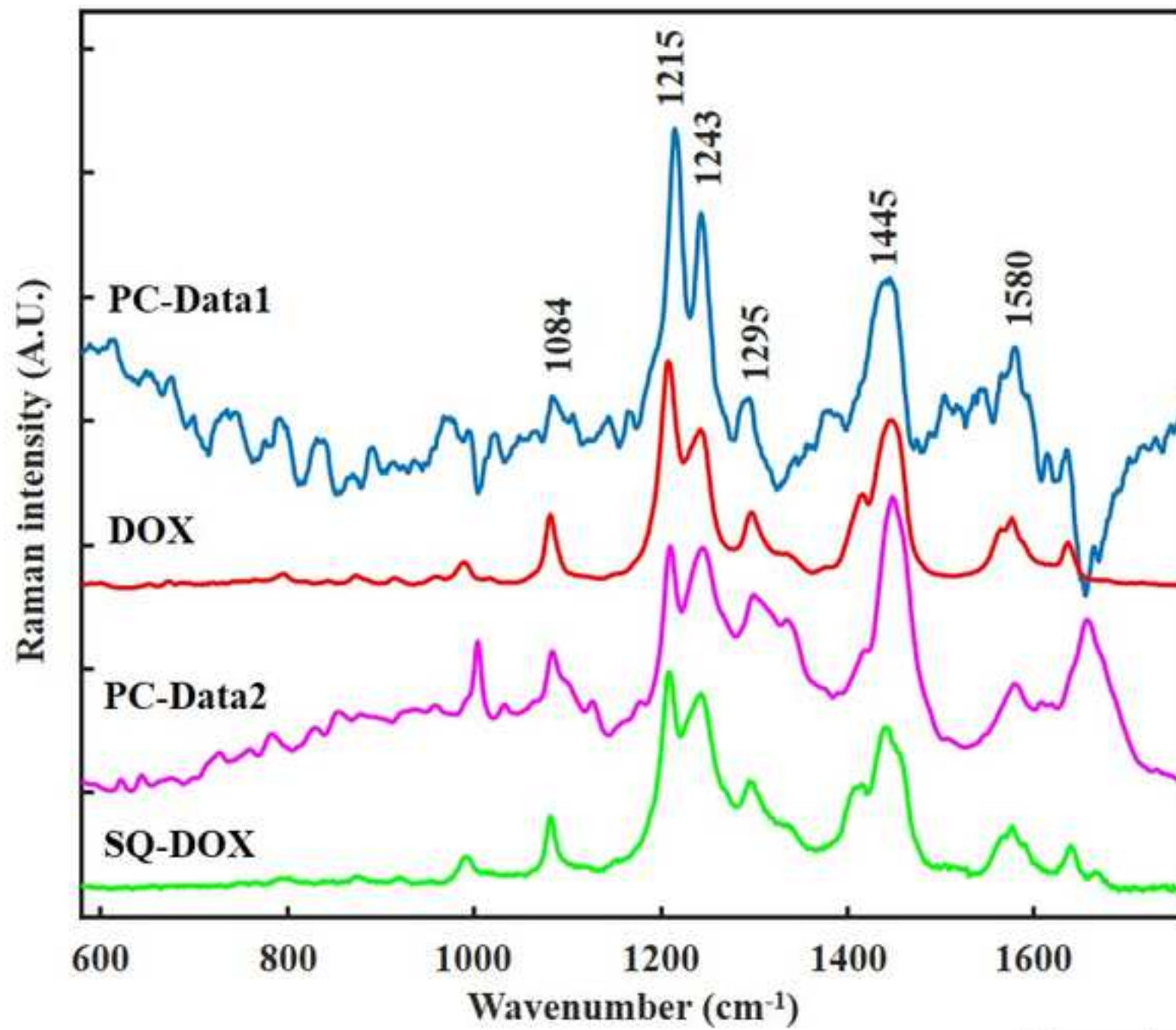


Figure 8

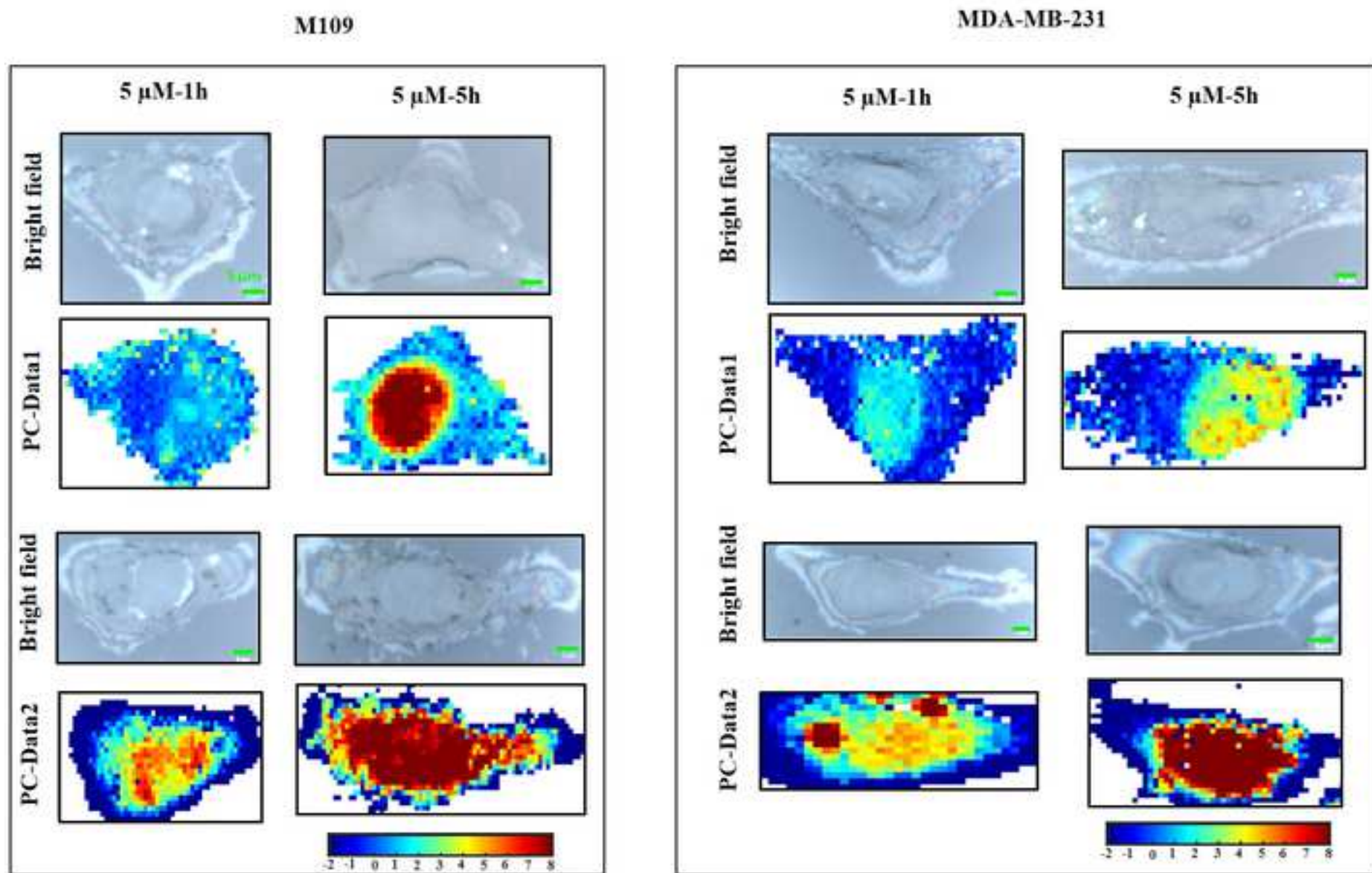


Figure 9



Click here to access/download
Supplementary Material
Supplementary information 1.pdf



NANOMEDICINE: NBM

<http://www.nanomedjournal.com/>

<http://www.ees.elsevier.com/nano/>

nbnm.journaloffice@gmail.com

AUTHORSHIP AGREEMENT


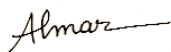

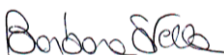




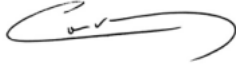
Must be signed by ALL authors
Scan and upload with your submission.

In accordance with the Authorship and Contributorship policy available at www.icmje.org, the undersigned certify that each participant: 1) made substantial contributions to conception and design, or acquisition of data, or analysis and interpretation of data; 2) drafted the article or revised it critically for important intellectual content; and 3) gives final approval of the submitted manuscript, revised versions, and version to be published. Authors should meet conditions 1, 2, and 3.

Manuscript # **JN2020930**_____

Title: Investigation of squalene-doxorubicin distribution and interactions within single cancer cell using Raman microspectroscopy

Signatures (All author names must be typed/printed next to signature. If more lines are needed, attach photocopies of this form.)

Signature		Typed name	Hassan Rammal	Date	09/03/2021
Signature		Typed name	Almar Al Assaad	Date	09/03/2021
Signature		Typed name	Franco Dosio	Date	09/03/2021
Signature		Typed name	Barbara Stella	Date	09/03/2021
Signature		Typed name	Andrei Maksimenko	Date	09/03/2021
Signature		Typed name	Simona Mura	Date	09/03/2021
Signature		Typed name	Laurence Van Gulick	Date	09/03/2021
Signature		Typed name	Maïté Callewaert	Date	09/03/2021
Signature		Typed name	Didier Desmaële	Date	09/03/2021
Signature		Typed name	Patrick Couvreur	Date	09/03/2021

Signature



Typed name **Hamid Morjani**

Date 09/03/2021

Signature



Typed name **Abdelilah Beljebbar**

Date 09/03/2021

Note: This is not a transfer of copyright. The publisher will provide a copyright form.

CRedit author statement

Hassan Rammal: Methodology and data acquisition, Data analysis and manuscript writing.

Almar Al Assaad: synthesis and characterization of nanoparticles, Methodology and data acquisition, Data analysis and manuscript writing.

Franco Dosio: synthesis and characterization of nanoparticles.

Barbara Stella: synthesis and characterization of nanoparticles.

Andrei Maksimenko: synthesis and characterization of nanoparticles.

Simona Mura: Discussion and revision.

Laurence Van Gulick: Methodology and data acquisition.

Maïté Callewaert: synthesis and characterization of nanoparticles.

Didier Desmaële: Discussion and revision.

Patrick Couvreur: Conception and design, Discussion and revision.

Hamid Morjani: Conception and design, Data analysis and manuscript writing.

Abdelilah Beljebbar: Conception and design, Methodology and data acquisition, Data analysis and manuscript writing.

- Squalenoyl-doxorubicin nanomedicine improve the efficacy of doxorubicin *in vivo*.
- Raman microspectroscopy allows characterization of such strategy at cellular level.
- Cellular distribution and molecular information on chemotherapeutic agents.
- Biochemical changes induced by drug treatment.